

26. Cooke KR, Kobzik L, Martin TR, et al. An experimental model of idiopathic pneumonia syndrome after bone marrow transplantation: I. The roles of minor H antigens and endotoxin. *Blood*. 1996; 88(8):3230-3239.
27. Kaplan DH, Anderson BE, McNiff JM, Jain D, Shlomchik MJ, Shlomchik WD. Target antigens determine graft-versus-host disease phenotype. *J Immunol*. 2004;173(9):5467-5475.
28. Mucida D, Park Y, Kim G, et al. Reciprocal TH17 and regulatory T cell differentiation mediated by retinoic acid. *Science*. 2007;317(5835):256-260.
29. Klemann C, Raveney BJ, Klemann AK, et al. Synthetic retinoid Am80 inhibits Th17 cells and ameliorates experimental autoimmune encephalomyelitis. *Am J Pathol*. 2009;174(6):2234-2245.
30. Chu YW, Gress RE. Murine models of chronic graft-versus-host disease: insights and unresolved issues. *Biol Blood Marrow Transplant*. 2008;14(4):365-378.
31. Mangan PR, Harrington LE, O'Quinn DB, et al. Transforming growth factor-beta induces development of the T(H)17 lineage. *Nature*. 2006; 441(7090):231-234.
32. Yi T, Chen Y, Wang L, et al. Reciprocal differentiation and tissue-specific pathogenesis of Th1, Th2, and Th17 cells in graft-versus-host disease. *Blood*. 2009;114(14):3101-3112.
33. Yi T, Zhao D, Lin CL, et al. Absence of donor Th17 leads to augmented Th1 differentiation and exacerbated acute graft-versus-host disease. *Blood*. 2008;112(5):2101-2110.
34. Kappel LW, Goldberg GL, King CG, et al. IL-17 contributes to CD4-mediated graft-versus-host disease. *Blood*. 2009;113(4):945-952.
35. Carlson MJ, West ML, Coghill JM, Panoskaltis-Mortari A, Blazar BR, Serody JS. In vitro-differentiated TH17 cells mediate lethal acute graft-versus-host disease with severe cutaneous and pulmonary pathologic manifestations. *Blood*. 2009;113(6):1365-1374.
36. Shustov A, Luzina I, Nguyen P, et al. Role of perforin in controlling B-cell hyperactivity and humoral autoimmunity. *J Clin Invest*. 2000;106(6): R39-R47.
37. Hill GR, Oliver SD, Kuns RD, et al. Stem cell mobilization with G-CSF induces type 17 differentiation and promotes scleroderma. *Blood*. 2010; 116(5):819-828.
38. Chen X, Das R, Komorowski R, van Snick J, Uyttenhove C, Drobyski WR. Interleukin 17 is not required for autoimmune-mediated pathologic damage during chronic graft-versus-host disease. *Biol Blood Marrow Transplant*. 2010;16(1):123-128.
39. Chen X, Vodanovic-Jankovic S, Johnson B, Keller M, Komorowski R, Drobyski WR. Absence of regulatory T-cell control of TH1 and TH17 cells is responsible for the autoimmune-mediated pathology in chronic graft-versus-host disease. *Blood*. 2007;110(10):3804-3813.
40. Dander E, Balduzzi A, Zappa G, et al. Interleukin-17-producing T-helper cells as new potential player mediating graft-versus-host disease in patients undergoing allogeneic stem-cell transplantation. *Transplantation*. 2009;88(11):1261-1272.
41. Ochs LA, Blazar BR, Roy J, Rest EB, Weisdorf DJ. Cytokine expression in human cutaneous chronic graft-versus-host disease. *Bone Marrow Transplant*. 1996;17(6):1085-1092.
42. Ritchie D, Seconi J, Wood C, Walton J, Watt V. Prospective monitoring of tumor necrosis factor alpha and interferon gamma to predict the onset of acute and chronic graft-versus-host disease after allogeneic stem cell transplantation. *Biol Blood Marrow Transplant*. 2005;11(9):706-712.
43. Korholz D, Kunst D, Hempel L, et al. Decreased interleukin 10 and increased interferon-gamma production in patients with chronic graft-versus-host disease after allogeneic bone marrow transplantation. *Bone Marrow Transplant*. 1997;19(7): 691-695.
44. Imanguli MM, Swaim WD, League SC, Gress RE, Pavletic SZ, Hakim FT. Increased T-bet+ cytotoxic effectors and type I interferon-mediated processes in chronic graft-versus-host disease of the oral mucosa. *Blood*. 2009;113(15):3620-3630.
45. Korn T, Bettelli E, Gao W, et al. IL-21 initiates an alternative pathway to induce proinflammatory T(H)17 cells. *Nature*. 2007;448(7152):484-487.
46. Axtell RC, Xu L, Barnum SR, Raman C. CD5-CK2 binding/activation-deficient mice are resistant to experimental autoimmune encephalomyelitis: protection is associated with diminished populations of IL-17-expressing T cells in the central nervous system. *J Immunol*. 2006;177(12): 8542-8549.
47. Sato A, Watanabe K, Kaneko K, et al. The effect of synthetic retinoid, Am80, on T helper cell development and antibody production in murine collagen-induced arthritis. *Mod Rheumatol*. 2010; 20(3):244-251.
48. Tawara I, Maeda Y, Sun Y, et al. Combined Th2 cytokine deficiency in donor T cells aggravates experimental acute graft-vs-host disease. *Exp Hematol*. 2008;36(8):988-996.
49. Tobita T, Takeshita A, Kitamura K, et al. Treatment with a new synthetic retinoid, Am80, of acute promyelocytic leukemia relapsed from complete remission induced by all-trans retinoic acid. *Blood*. 1997;90(3):967-973.

blood

2012 120: 223-231
Prepublished online April 24, 2012;
doi:10.1182/blood-2011-12-401166

Graft-versus-host disease disrupts intestinal microbial ecology by inhibiting Paneth cell production of α -defensins

Yoshihiro Eriguchi, Shuichiro Takashima, Hideyo Oka, Sonoko Shimoji, Kiminori Nakamura, Hidetaka Uryu, Shinji Shimoda, Hiromi Iwasaki, Nobuyuki Shimono, Tokiyoshi Ayabe, Koichi Akashi and Takanori Teshima

Updated information and services can be found at:
<http://bloodjournal.hematologylibrary.org/content/120/1/223.full.html>

Articles on similar topics can be found in the following Blood collections
Transplantation (1853 articles)

Information about reproducing this article in parts or in its entirety may be found online at:
http://bloodjournal.hematologylibrary.org/site/misc/rights.xhtml#repub_requests

Information about ordering reprints may be found online at:
<http://bloodjournal.hematologylibrary.org/site/misc/rights.xhtml#reprints>

Information about subscriptions and ASH membership may be found online at:
<http://bloodjournal.hematologylibrary.org/site/subscriptions/index.xhtml>

Blood (print ISSN 0006-4971, online ISSN 1528-0020), is published weekly by the American Society of Hematology, 2021 L St, NW, Suite 900, Washington DC 20036.
Copyright 2011 by The American Society of Hematology; all rights reserved.



Graft-versus-host disease disrupts intestinal microbial ecology by inhibiting Paneth cell production of α -defensins

Yoshihiro Eriguchi,¹ Shuichiro Takashima,¹ Hideyo Oka,¹ Sonoko Shimoji,¹ Kiminori Nakamura,² Hidetaka Uryu,¹ Shinji Shimoda,¹ Hiromi Iwasaki,³ Nobuyuki Shimonono,¹ Tokiyoshi Ayabe,² Koichi Akashi,^{1,3} and Takanori Teshima³

¹Department of Medicine and Biosystemic Science, Kyushu University Graduate School of Medical Science, Fukuoka, Japan; ²Department of Cell Biological Science, Graduate School of Life Science, Faculty of Advanced Life Science, Hokkaido University, Sapporo, Japan; and ³Center for Cellular and Molecular Medicine, Kyushu University Graduate School of Medical Science, Fukuoka, Japan

Allogeneic hematopoietic stem cell transplantation (SCT) is a curative therapy for various hematologic disorders. Graft-versus-host disease (GVHD) and infections are the major complications of SCT, and their close relationship has been suggested. In this study, we evaluated a link between 2 complications in mouse models. The intestinal microbial communities are actively regulated by Paneth cells through their secretion of antimicrobial peptides, α -defensins. We discovered that Paneth cells are targeted by

GVHD, resulting in marked reduction in the expression of α -defensins, which selectively kill noncommensals, while preserving commensals. Molecular profiling of intestinal microbial communities showed loss of physiologic diversity among the microflora and the overwhelming expansion of otherwise rare bacteria *Escherichia coli*, which caused septicemia. These changes occurred only in mice with GVHD, independently on conditioning-induced intestinal injury, and there was a significant correlation between alteration

in the intestinal microbiota and GVHD severity. Oral administration of polymyxin B inhibited outgrowth of *E coli* and ameliorated GVHD. These results reveal the novel mechanism responsible for shift in the gut flora from commensals toward the widespread prevalence of pathogens and the previously unrecognized association between GVHD and infection after allogeneic SCT. (*Blood*. 2012;120(1):223-231)

Introduction

Allogeneic hematopoietic stem cell transplantation (SCT) is a curative therapy for hematologic malignant tumors, bone marrow failure, and congenital metabolic disorders. Graft-versus-host disease (GVHD) and related infections are major obstacles to SCT, and their close relationship has been indicated in clinical settings. Septicemia is the most life-threatening infection after allogeneic SCT and gram-negative rods are the most dominant pathogens of septicemia, whereas incidence of drug-resistant enterococci infection increase in neutropenic patients colonized with these bacteria in some centers.¹ GVHD is one of the major predisposing factors for the development of septicemia.² Since the pioneering works of van Bekkum³ and others in the 1960s-1970s, interaction between intestinal flora and GVHD has been suggested.³⁻⁶

We recently demonstrated that intestinal stem cells (ISCs), which are essential to repair damaged intestinal epithelium, are targeted by GVHD.⁷ Recently, Paneth cells located besides ISCs within the crypts are identified as niche for ISCs.⁸ In addition, Paneth cells are essential regulators of the composition of intestinal microbiota by secreting antimicrobial peptides, α -defensins, which provide broad-spectrum antimicrobial properties by pore formation in the bacterial cell walls.⁹⁻¹¹ The intestine, which is the major interface between the environment and the host, is an open ecologic system that is colonized by at least 1000 distinct bacterial species, of which more than 80% are nonculturable.¹²⁻¹⁴ Accurate identification of species in the gut microbiota requires culture-independent, molecular profiling methods. Firmicutes and Bacteroidetes make

up approximately 90% of the intestinal microbiota.^{12,15} These commensals are rarely pathogenic and instead make several essential contributions to human physiology and health.^{12,13,15,16} In contrast, Gammaproteobacteria such as *Escherichia coli*, which have a gram-negative cell wall make up a small proportion of the microbiota.¹⁷ A recent study showed an increase in gram-negative *Enterobacteriaceae* family members including *E coli* among the intestinal microbiota after allogeneic bone marrow transplantation (BMT) in mice.¹⁸ It remains unclear why they are most frequent pathogens in patients with intestinal GVHD, although the role of systemic immunosuppression and use of antibiotics has been well appreciated.¹⁹

In this study, we focused on Paneth cells and evaluated the possible mechanistic links between GVHD and infection in mouse models of BMT. We found that GVHD targets Paneth cells and causes subsequent impairment of antimicrobial peptide secretion, leading to marked loss of diversity among the intestinal microflora. This results in shift in the gut flora from commensal microorganisms toward the widespread prevalence of gram-negative bacteria and development of bloodstream infection.

Methods

Mice

Female C57BL/6 (B6: H-2^b), B6D2F1 (H-2^{b/d}), B6C3F1 (H-2^{b/k}), B6-Ly5.1 (H-2^b, CD45.1⁺), and C3H.Sw (H-2^b) mice were purchased from Charles

Submitted December 25, 2011; accepted April 22, 2012. Prepublished online as *Blood* First Edition paper, April 24, 2012; DOI 10.1182/blood-2011-12-401166.

There is an Inside *Blood* commentary on this article in this issue.

The publication costs of this article were defrayed in part by page charge payment. Therefore, and solely to indicate this fact, this article is hereby marked "advertisement" in accordance with 18 USC section 1734.

© 2012 by The American Society of Hematology

River Japan, KBT Oriental, or Japan SLC. All animal experiments were performed under the auspices of the Institutional Animal Care and Research Advisory Committee.

BMT

Mice were transplanted as previously described.²⁰ In brief, after lethal x-ray total body irradiation (TBI) delivered in 2 doses at 4-hour intervals, mice were intravenously injected with 5×10^6 T-cell depleted bone marrow (TCD-BM) cells with or without 2×10^6 splenic T cells on day 0. Isolation of T cells and T-cell depletion were performed using the T-cell isolation kit and anti-CD90 microBeads, respectively, and the AutoMACS (Miltenyi Biotec) according to the manufacturer's instructions. In some experiments, unirradiated B6D2F1 mice were intravenously injected with 12×10^7 splenocytes.⁷ Mice were maintained in specific pathogen-free conditions and received normal chow and autoclaved hyperchlorinated water (Ph 4) for the first 3 weeks after BMT and filtered water thereafter. Polymyxin B (Calbiochem) diluted in water was administered by daily oral gavage at a dose of 100 mg/kg from day -4 until day 28 after BMT. Survival after BMT was monitored daily and the degree of clinical GVHD was assessed weekly by a scoring system which sums changes in 5 clinical parameters: weight loss, posture, activity, fur texture, and skin integrity (maximum index = 10) as previously described.²⁰

Histologic and immunohistochemical analysis

For pathologic analysis, samples of the small intestine were fixed in 10% neutral-buffered formalin, embedded in paraffin, sectioned, slide mounted, and stained with H&E. Immunohistochemistry was performed as described²¹ using rabbit anti-lysozyme (Dako) and rabbit anti-defensin1. Histofine simple stain MAX PO (Rat) kits and subsequently diaminobenzidine (DAB) solution (Nichirei Biosciences) was used to generate brown-colored signals. Slides were then counterstained with hematoxylin. Pictures from tissue sections were taken at room temperature using a digital camera (DP72; Olympus) mounted on a microscope (BX51; Olympus). Acute GVHD was assessed by detailed histopathologic analysis using a semiquantitative scoring system.²²

Preparation and analysis of isolated mouse crypts

Individual crypts were isolated from the small intestine as previously described.²³ Isolated crypts were fixed with 2% paraformaldehyde in PBS for 20 minutes and permeabilized with 0.2% Triton X-100 in PBS for 5 minutes. Crypts were incubated for 1 hour with fluorescein isothiocyanate-conjugated anti-lysozyme (10 μ g/mL; Dako), washed 3 times in PBS, followed by incubation for 1 hour with Alexa Fluor 594-conjugated phalloidin (1 U/mL; Invitrogen). Tetramethyl 4,6-diamidino-2-phenylindole (DAPI; 5 μ g/mL; Invitrogen) was used to stain the nucleus. Samples were mounted in aqua poly/mount (Polysciences) and examined with a confocal laser-scanning microscope (LSM510; Carl Zeiss).

Enzyme-linked immunosorbent assay

The limulus amoebocyte lysate assay QCL-1000 (Lonza) was performed according to the manufacturer's instructions to determine the serum level of lipopolysaccharide (LPS) with a sensitivity of 0.1 EU/mL. All units expressed are relative to the United States reference standard EC-2.

Quantitative real-time PCR analysis

Total RNA was purified using the RNeasy Kit (QIAGEN). cDNA was synthesized using a QuantiTect reverse transcription kit (QIAGEN). Polymerase chain reactions (PCRs) and analyses were performed with ABI PRISM 7900HT SDS 2.1 (Applied Biosystems) using TaqMan universal PCR master mix (Applied Biosystems), and TaqMan gene expression assays (Defa1: Mm02524428_g1, Defa4: Mm00651736_g1, Defa5: Mm00651548_g1, Defa21/Defa22: Mm04206099_gH, Defcr-rs1: Mm00655850_m1, Lyz1: Mm00657323_m1, and Gapdh: Mm99999915_g1; Applied Biosystems). The relative amount of each mRNA was determined using the standard curve method and was normalized to the level of GAPDH in each sample.

Total fecal bacterial DNA extraction

Total DNA was isolated from fecal pellets using a QIAamp DNA stool mini kit (QIAGEN) with bead beating treatment during the cell-lysis step. Briefly, fresh fecal pellets were collected from individual mice; 0.5 g baked 0.1 mm zirconia/silica beads (Biospec Products) and ASL buffer were added to each aliquot. Fecal samples with ASL buffer were incubated at 95°C, and samples were processed for 1 minute at speed 5.5 on Fastprep system (Qbiogene).²⁴

PCR amplification of 16S rRNA gene

Bacterial 16S ribosomal RNA (rRNA) genes were amplified with bacterial-universal primers, 27F (5'-AGAGTTTGATCCTGGCTCAG-3') labeled at the 5' end with 6-carboxyfluorescein (6-FAM) and 1492R (5'-GGTTACCTTGT TACGACTT-3').²⁵ PCR amplification was performed using *EX Taq* (Takara Bio) and the following program: 3 minutes of denaturation at 95°C, 30 cycles of 0.5 minute at 95°C, 0.5 minute at 50°C, 1.5 minute at 72°C, and a final 10 minutes extension step at 72°C in a BiometraT3 thermocycler (Biometra). Amplicons were purified using a QIAquick PCR Purification kit (QIAGEN).

Restriction fragment length polymorphism (RFLP) analysis

The purified DNA products (3 μ L) were digested with 10 U of either *Hha*I or *Msp*I (Takara Bio) in a total volume of 10 μ L at 37°C for 3 hours. The restriction digest products (2 μ L) were mixed with 10 μ L deionized formamide and 0.5 μ L GeneScan-1200 LIZ standard (Applied Biosystems). The samples were denatured at 95°C for 2 minutes, followed by rapid chilling on ice. The fluorescently labeled fragments (T-RFs) were separated by size on an ABI 3130 genetic analyzer (Applied Biosystems). The electropherograms were analyzed with GeneMapper Version 4.0 software (Applied Biosystems), and the fragment sizes were estimated using the Local Southern method. Each unique RFLP pattern was designated as an operational taxonomic unit (OTU). OTUs with a peak area of less than 0.5% of the total area were excluded from the analysis. Proportion of *E coli* was defined as the ratio of area of OTU for *E coli* to total areas of OTUs. Diversity of the microbial community corresponding to the RFLP banding pattern was calculated using the Simpson index of diversity 1-D ($D = \sum \pi_i^2$)²⁶ and Shannon diversity index H' ($H' = -\sum \pi_i \ln(\pi_i)$)²⁷ and where π_i is the proportion of total number of species made up of its species.

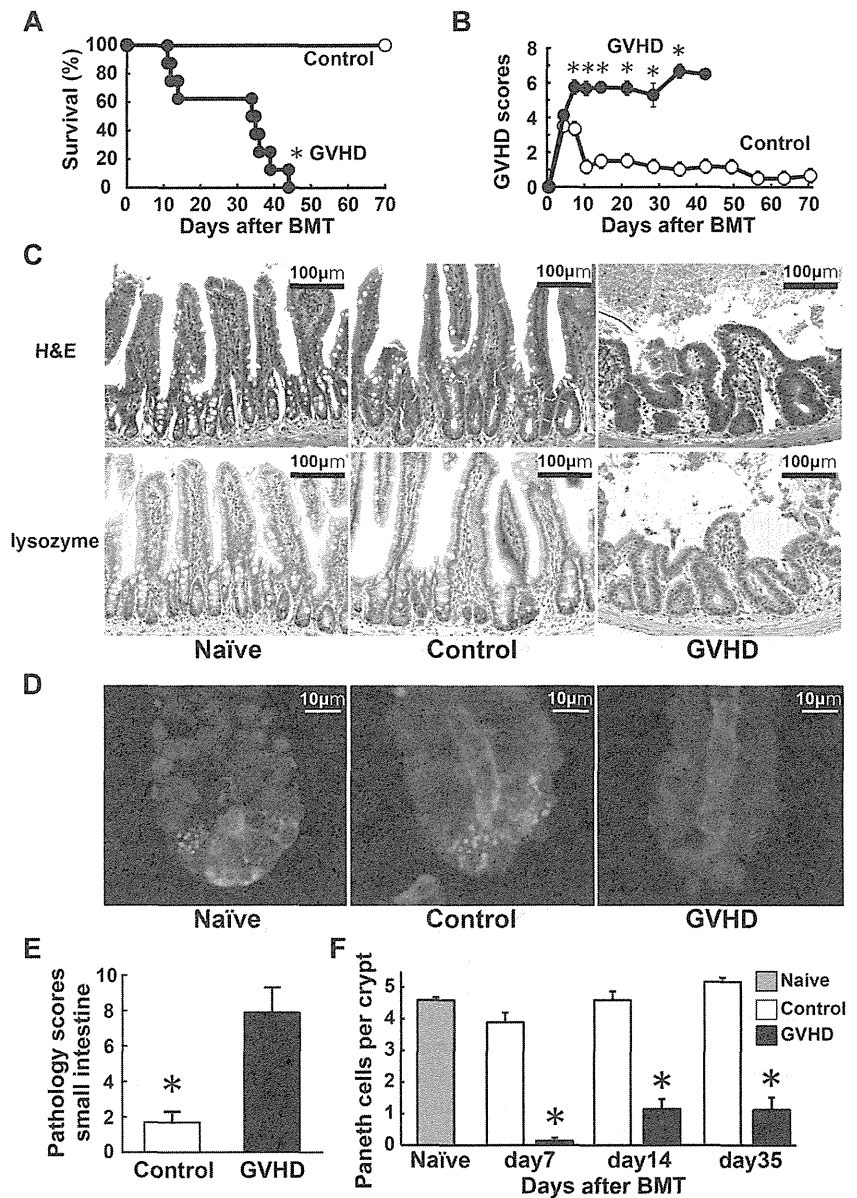
Cloning and sequencing analysis

Internal region of the 16S rRNA genes were amplified using 27F and 806R (5'-GGACTACCAGGGTATCTAAT-3') primers, and were transformed using TOPO TA Cloning Kit with TOP10 *E coli* (Invitrogen). The nucleotide sequences of inserts were determined using the M13 forward and reverse primers. All sequences were examined for possible chimeric artifacts by the Chimera check with Bellerophon Version 3. After eliminating chimeric sequences, the partial 16S rRNA sequences were compared with the sequences in the Ribosomal Database Project and GenBank, using the BLAST program (<http://www.ncbi.nlm.nih.gov/BLAST/>). Cloned sequences were identified as representing the species or phylotype of the sequence with the highest matching score. Sequences with less than 98% identity with a GenBank sequence were defined as a new phylotype. In addition, we checked whether the sequenced clones had the correct T-RFs compared with the sequence information.

Microbiologic analysis of bacterial translocation

The livers and mesenteric lymph nodes (mLNs) isolated from mice that had received transplants were removed aseptically and homogenized in 1 mL saline. Then, 500 μ L of homogenate was transferred into a tube containing 4.5 mL of saline and used to perform 4 serial dilutions. From this dilution, 100 μ L aliquots were cultured aerobically on blood agar and LB agar plates (Difco) for 24 hours at 37°C in room air supplemented with 10% CO₂. Colony-forming units (CFUs) were counted and adjusted per organ. Bacteria were identified by biochemical profiles.

Figure 1. Paneth cell injury in GVHD. Lethally irradiated B6D2F1 mice were transplanted with 5×10^6 TCD BM cells without (control group, $n = 6$) or with 2×10^6 T cells (GVHD group, $n = 12$) from MHC-mismatched B6 donors on day 0. (A-B) Survival (A) and clinical GVHD scores (B) means \pm SE are shown. Data from 2 independent experiments were combined. (C-F) Small intestines were isolated from mice 7 days after BMT. (C) Top panels: histology of the small intestine stained with H&E. Bottom panels: Lysozyme staining (brown). Magnification: $100\times$. Bars, $100 \mu\text{m}$. (D) Confocal cross-sectioning of the isolated small intestinal crypt. Lysozyme (green) is expressed by Paneth cells. Tetramethyl DAPI (blue) stains the nucleus and phalloidin (red) stains F-actin. Magnification: $1000\times$. Bars, $10 \mu\text{m}$. (E) Pathology scores of the small intestine (mean \pm SE, $n = 3-6$ / group). (F) Quantification of Paneth cells per crypt (mean \pm SE, $n = 3-6$ / group; $*P < .05$).



Statistical analysis

Mann-Whitney *U* tests were used to compare data, the Kaplan-Meier product limit method was used to obtain survival probability, and the log-rank test was applied to compare survival curves. To determine the statistically significant correlation, the Spearman rank correlation coefficient (*R*) was adopted. All tests were performed with SigmaPlot Version 10.0 software. $P < .05$ was considered statistically significant.

Accession numbers

Sequence data are available in the GenBank (<http://www.ncbi.nih.gov/genbank>) under the accession number 1509996.

Results

Paneth cell damage and decreased expression of α -defensins in GVHD

We evaluated whether Paneth cells could be damaged during GVHD. Lethally irradiated B6D2F1 (H-2^{b/d}) mice received 5×10^6 TCD-BM

cells (control group) or these cells plus 2×10^6 T cells (GVHD group) from major histocompatibility complex (MHC)-mismatched B6 (H-2^b) donors on day 0. The allogeneic animals developed severe GVHD and all of these mice died within 50 days after BMT, whereas all TCD-BM controls survived through this period (Figure 1A). The surviving allogeneic animals showed significantly more severe signs of GVHD than controls, as assessed by clinical GVHD scores²⁰ (Figure 1B). Pathologic analysis of the small intestine 7 days after BMT showed mostly normal architecture in controls, whereas severe blunting of villi and inflammatory infiltration were observed in the GVHD group (Figure 1C). Paneth cells, which are typically identified microscopically by their location in the crypts and by the large granules occupying most of their cytoplasm, were hardly observed in the GVHD group. Immunohistochemical analysis for lysozyme, which indicates the presence of Paneth cells, confirmed loss of Paneth cells in the GVHD group, but not in controls (Figure 1C). Confocal cross-sectioning of individual crypts isolated from the small intestine further confirmed Paneth cell loss in these mice (Figure 1D). In mice with GVHD, GVHD pathology scores were significantly higher (Figure 1E), whereas numbers of Paneth cells

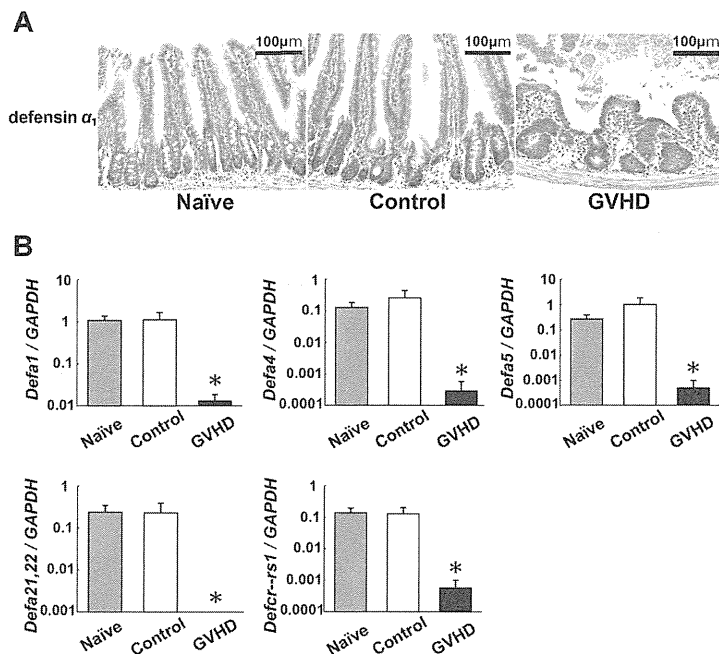


Figure 2. Decreased expression of Paneth cell–derived α -defensins in GVHD. Lethally irradiated B6D2F1 mice were transplanted with 5×10^6 TCD BM without (control group) or with (GVHD group) 2×10^6 T cells from B6 donors. Small intestines were isolated from mice 7 days after BMT. (A) Immunohistochemical staining for defensin α_1 (brown). Magnification: 100 \times . Bars, 100 μ m. (B) RNA was extracted from samples and quantitative real-time PCR analysis for enteric defensins including *Defa1*, *Defa4*, *Defa5*, *Defa21,22*, and *Defcr-rs1* was performed ($n = 6$ / group). Data are representative of 2 similar experiments and are shown as mean \pm SE (* $P < .05$).

were significantly and constantly lower compared with those in controls after BMT (Figure 1F).

α -Defensins are the major antimicrobial peptides produced by Paneth cells.²³ We evaluated the expression levels of enteric defensin families in the small intestines. Defensin α_1 expression was limited in Paneth cells in the crypts of naive mice (Figure 2A). Expression of defensin α_1 was preserved in controls 7 days after BMT but was severely suppressed in mice with GVHD. Quantitative real-time PCR analysis of the terminal ileum confirmed the reduced expression of *defensin- α_1* (*Defa1*) and other enteric defensin family members, including *Defa5*, *Defa21,22*, and *defensin α -related sequence 1* (*Defa-rs1*) in the small intestine of GVHD mice (Figure 2B). These results demonstrate that GVHD targets Paneth cells and limits the expression of Paneth cell–derived defensin family members.

Perturbation of normal intestinal microbiota in GVHD

Paneth cell–derived α -defensins are essential regulators of the microbiota composition in the intestine.¹¹ α -defensins have selective bactericidal activity against noncommensals, whereas exhibiting minimal bactericidal activity against commensals.^{28,29} We therefore hypothesized that the reduced expression of α -defensins results in dysbiosis in the intestinal microbial community. To test this hypothesis, we evaluated changes in the gut flora during the course of GVHD in a B6 \rightarrow B6D2F1 murine model of BMT without administering any antibiotic or immunosuppressive drugs. Before and after BMT, fecal pellets were collected from each mouse once per week. The composition of the intestinal microflora was determined by RFLP analysis of bacteria-specific 16S rRNA genes that were constructed from each sample of fecal pellets.^{30,31} Representative RFLP analysis is shown in Figure 3A. Each unique RFLP pattern is designated by an OTU that corresponds to specific species of bacteria. The peak height of each OTU indicates its relative quantity among the intestinal microflora and the number of OTUs indicates the diversity of flora. Before BMT, multiple OTUs were observed with little interindividual variation among the RFLP patterns (Figure 3A left panels). Seven days after BMT, numbers of

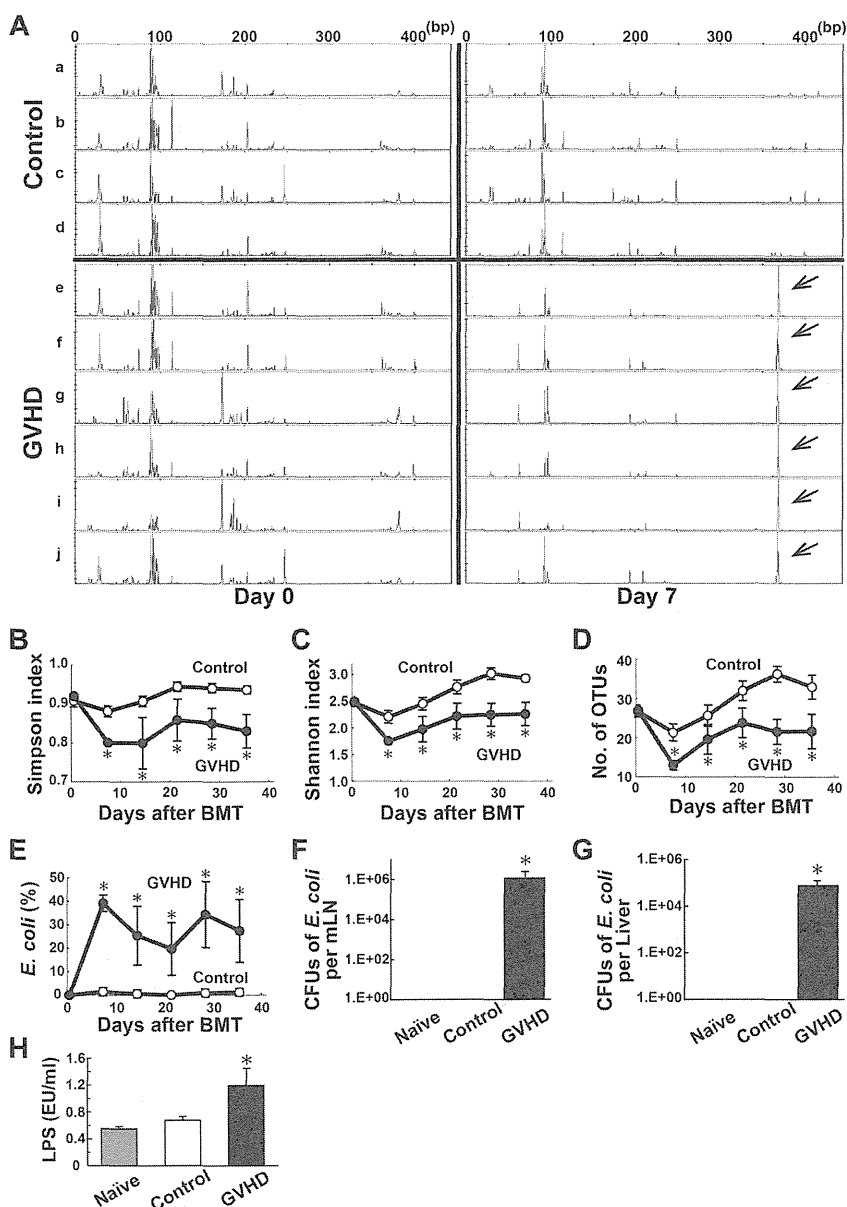
OTUs were slightly decreased with little changes in the RFLP patterns in controls (Figure 3A right top panels); however, in the mice with GVHD, the number of OTUs decreased and the peak heights of OTUs were markedly reduced, with the exception of an aberrantly high peak at 368 bp (Figure 3A right bottom panels). Sequence analysis of subclones from a representative animal from GVHD group showed that proportions of both Firmicutes and Bacteroidetes, which are the major enteric commensals,^{12,15} were decreased in mice with GVHD on day 7 compared with those before BMT (Firmicutes; 22.9% vs 52.1%, Bacteroidetes; 2.1% vs 13.5%, respectively).

These compositional changes in the intestinal microflora were consistently observed in all mice with GVHD. Diversity of the microbial community, which corresponds to the RFLP banding patterns, was significantly reduced in mice with GVHD at all time points, as assessed by the Simpson index of diversity,²⁶ Shannon diversity index,²⁷ and the number of OTUs counted (Figure 3B-D).

Overwhelming outgrowth of *E coli* in mice with GVHD

A single high peak at 368bp was noted in mice with GVHD (Figure 3A arrows). To identify the bacteria included at this OTU, plasmid DNA from the corresponding clone was purified. DNA sequencing showed a high similarity to 16S rRNA from *E coli* with a similarity rate of more than 99.5%. The proportion of *E coli* in the microbiota, which was defined as the ratio of the area of OTU for *E coli* to the total areas of all OTUs, was dramatically higher 7 days after BMT and remained higher in mice with GVHD throughout the entire observation period; however, *E coli* remained to be a small portion of the microbial population in controls (Figure 3E). Next, we evaluated whether the high levels of *E coli* in the intestine could be associated with the development of systemic infection in mice with GVHD. Seven days after BMT, mLNs and livers were harvested. *E coli* was identified from samples taken from mice with GVHD, but not the controls. The number of CFUs of *E coli* was significantly higher in the mLNs and liver of mice with GVHD than those in controls (Figure 3F-G). Serum LPS levels were also significantly higher in mice with GVHD than in controls (Figure 3H).

Figure 3. Perturbation of normal intestinal microbiota in GVHD. Fecal pellets were collected before and after a B6 → B6D2F1 BMT weekly and intestinal microbiota was characterized by RFLP analysis of 16S rRNA gene libraries constructed from each sample of fecal pellets and digested with *HhaI* (n = 6 / group). (A) Representative RFLP patterns are shown in control group (a-d) and GVHD group (e-j). Left panels indicate before BMT; right panels, 7 days after BMT. Arrows indicate an OTU for *Escherichia coli*. (B-D) Time course changes in flora diversity after BMT determined by using Simpson index (B), Shannon index (C), and numbers of OTUs (D). (E) Time course changes in the proportion of *E. coli*. (F-G) Samples of mLNs and liver were harvested on day 7 and CFUs of *E. coli* were enumerated by the culture-based and microbiologic identification method. (H) Serum LPS levels on day 7. Data are representative of 3 similar experiments and are shown as mean ± SE (*P < .05).



The composition of intestinal microflora in animals can differ depending on the environment and other factors.³² Therefore, we used mice purchased from multiple vendors; however, the resulting patterns of dysbiosis were similar, regardless of the origin source of the mice. In addition, we found similar changes in the intestinal microbiota of another haplotype, the mismatched B6 → B6C3F1 (H-2^{b/k}) model of BMT. Diversity of intestinal flora was lost with an outgrowth of *E. coli* 7 days after BMT and thereafter only in mice with GVHD (data not shown).

Association between changes in intestinal microbiota and GVHD severity

Further studies were conducted to determine whether there could be an association between the magnitude of changes observed in the intestinal flora and GVHD severity. Diversity of the flora, as determined by the Simpson index, Shannon index, and the number of OTUs was inversely correlated with GVHD severity (Figure

4A-C). On the other hand, the proportion of *E. coli* in the intestinal flora was positively correlated with GVHD severity (Figure 4D).

Delayed alteration in intestinal microbial diversity after MHC-matched BMT

To further confirm that our observations were not strain or model dependent, we evaluated whether the observed changes in the intestinal flora could be observed in a clinically relevant, MHC-matched, and minor histocompatibility antigen-mismatched C3H.Sw (H-2^b) → B6 (H-2^b) model of BMT, in which GVHD developed more slowly and was less severe compared with the MHC-mismatched models of GVHD (Figure 5A-B).³³ Again, normal microbial diversity was lost in mice with GVHD and *E. coli* levels were higher at 2 weeks after BMT and thereafter (Figure 5C-F). Thus, changes in the intestinal microbiota occurred more slowly in this model, at least compared with the MHC-mismatched model of GVHD; furthermore, the changes occurred in parallel with the

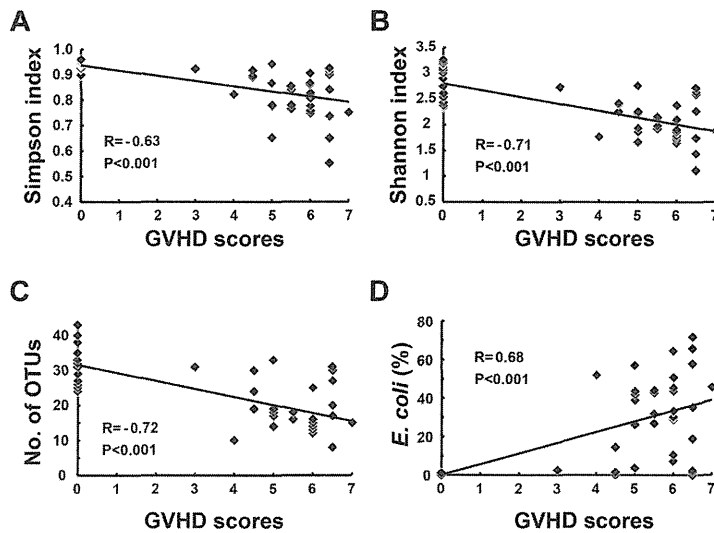


Figure 4. Correlation between the degree of flora changes and GVHD severity. Lethally irradiated B6D2F1 mice were transplanted with TCD BM with T cells from B6 donors (n = 6 / group). Fecal pellets were collected at day 0 and weekly thereafter and intestinal microbiota was characterized by RFLP analysis. Clinical GVHD scores and various parameters of the flora diversity and the proportion of *E coli* in the intestinal flora at various time points from each mice were plotted. Correlations of GVHD clinical scores and Simpson index (A), Shannon index (B), numbers of OTUs (C), and proportion of *E coli* (D). The regression line was plotted with all data. Data from 2 independent experiments were combined. R: correlation coefficient.

slower development of GVHD. It should be noted that normal flora diversity was recovered and *E coli* returned to a normally small population among the intestinal microbiota late after BMT, as GVHD severity reduced. No mortality was observed in allogeneic animals after regaining normal intestinal flora.

Loss of Paneth cells and the dysbiosis by a mechanism independent on conditioning

We addressed whether GVHD mediates Paneth cell injury and the alteration of the composition of the intestinal flora by a mechanism dependent on radiation-induced intestinal tract damage in the B6 → B6D2F1 BMT model without conditioning, as previously described.⁷ Unirradiated B6D2F1 mice were intravenously injected with 12×10^7 splenocytes from syngeneic or allogeneic B6 donors on day 0. In this model, GVHD occurred early after BMT at a peak around day 20 but was spontaneously improved (Figure 6A-C). Numbers of Paneth cells were markedly reduced 2 weeks after BMT but gradually returned to normal levels thereafter in allogeneic animals (Figure 6D). The changes in the intestinal microbiota occurred in parallel with the degree of GVHD severity and Paneth cell injury; normal microbial diversity was lost with the outgrowth of *E coli*, but was gradually restored later after BMT in allogeneic animals (Figure 6E-H).

Oral administration of antibiotics inhibited the outgrowth of *E coli* and ameliorated GVHD

Finally, we evaluated whether modifying the enteric flora using oral antibiotics could ameliorate GVHD. Lethally irradiated B6D2F1 mice were transplanted with 5×10^6 TCD BM cells with or without 2×10^6 T cells from B6-Ly5.1 (CD45.1⁺) donors. Polymyxin B (PMB), an antibiotic primarily effective against gram-negative bacteria, was administered by daily oral gavage at a dose of 100 mg/kg from day -4 until day 28 after BMT. Analysis of fecal pellets 7 days after BMT showed that the outgrowth of *E coli* was inhibited in mice treated with PMB compared with those treated with diluent (Figure 7A). PMB suppressed the outgrowth of *E coli* during PMB treatment; however, *E coli* levels increased after cessation of PMB treatment (Figure 7B). Notably, administration of PMB significantly reduced mortality and morbidity of GVHD (Figure 7C-D). Donor (CD45.1⁺) T-cell expansion (Figure 7E) and pathology scores of the small intestine (Figure 7F) were significantly reduced in PMB-treated mice compared with those in controls.

Discussion

Intestinal GVHD is critical for determining the outcome of allogeneic BMT. Paneth cells are essential regulators of the

Figure 5. Delayed impairment of the intestinal ecology after MHC-matched BMT. B6 mice were transplanted with 5×10^6 TCD BM without (control group) or with (GVHD group) 2×10^6 T cells from C3H.Sw donors after 12 Gy TBI (n = 6/group). (A-B) Survival (A) and clinical GVHD scores (B, mean ± SE) in control group and GVHD group. Data are representative of 3 similar experiments. (C-F) Fecal pellets were collected once per week after BMT and intestinal microflora was characterized by RFLP analysis of 16S rRNA genes constructed from each sample of fecal pellets and digested with *HhaI*. Time course changes in flora diversity determined by Simpson index (C), Shannon index (D), and numbers of OTUs (E). (F) Time course changes in the proportion of *E coli*. Data are representative of 3 similar experiments and are shown as mean ± SE (*P < .05).

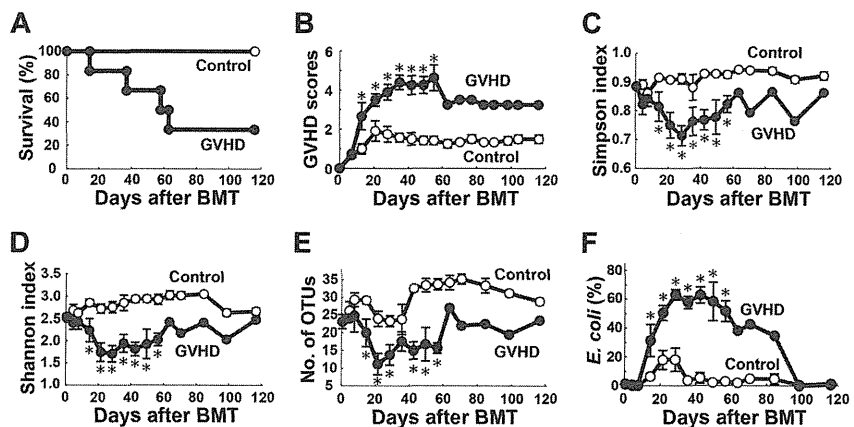
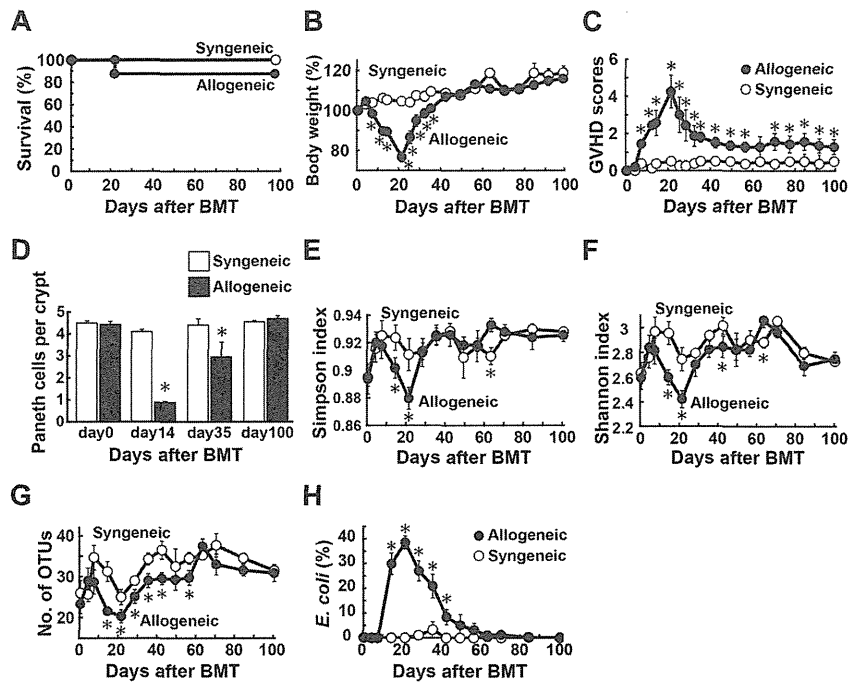


Figure 6. Paneth cell injury and the dysbiosis developed by a mechanism independent on conditioning. Unirradiated B6D2F1 mice were transplanted with 12×10^7 splenocytes from syngeneic or allogeneic MHC-mismatched B6 donors on day 0 ($n = 6$ /group). Survival (A), changes in body weight (B, mean \pm SE), clinical GVHD scores (C, mean \pm SE), and (D) quantification of Paneth cells per crypt in the small intestine were shown. (E-H) Fecal pellets were collected before and after BMT weekly and intestinal microbiota was characterized by RFLP analysis of 16S rRNA gene libraries constructed from each sample of fecal pellets and digested with *HhaI*. Time course changes in flora diversity determined by using Simpson index (E), Shannon index (F), numbers of OTUs (G), and the proportion of *E coli* (H). Data from 2 independent experiments were combined and are shown as mean \pm SE.



composition of commensal microbiota in the intestine, and they maintain the intestinal microbial environment by secreting various microbial peptides. In this study, we found that damage to Paneth cells by GVHD results in dramatically reduced expression of α -defensins in the small intestines and perturbed normal intestinal environment. These changes occurred in the absence of conditioning irradiation, thus indicating a mechanism dependent on allogeneic T-cell responses. However, Paneth cell loss occurred earlier and more prolonged in mice receiving irradiation than in unirradiated mice, suggesting that conditioning enhanced Paneth cell damage directly and indirectly by accelerating GVHD. The diversity of the intestinal microflora was lost with overwhelming expansion of specific bacteria, such as *E coli*, which are normally a very small proportion of the intestinal microbial communities. Paneth cells secrete α -defensins into the intestinal lumen within minutes after sensing gram-negative and gram-positive bacteria and their components, such as LPS, through activation of pattern recognition receptors.^{23,34} α -defensins are the most potent antimicrobial peptides and account for 70% of the bactericidal peptide activity released from Paneth cells.^{11,23} α -Defensins are released in the small bowel lumen and persist as intact and functional forms throughout the intestinal tract.³⁵ Thus, they shape the composition of the microbiota in the entire intestine. Importantly, α -defensins have selective bactericidal activity against noncommensals, such as *Salmonella enterica*, *E coli*, *Klebsiella pneumoniae*, and *Staphylococcus aureus*, although exhibiting minimal bactericidal activity against commensals.^{28,29} Such bacteria-dependent bactericidal activities of α -defensins are in tune with intestinal environment and may explain why the absence of α -defensins causes the alterations in the intestinal microbiota in GVHD. Because commensals have a profound influence on nutritional, physiologic, and metabolic function of the host,^{14,36,37} reduction of commensals may have ill effects on the host with GVHD. In this study, *E coli* was the dominant enteric microbe in mice with GVHD among multiple strains of mice. However, the dominant species may differ between studies because of the differences in several factors, including differences in the maintenance protocols used to feed and care for the experimental animals.³² Nonetheless, our study confirms and

further extends a recent study showing the intestinal flora change, with an increase in gram-negative *Enterobacteriaceae* family members including *E coli*, after allogeneic BMT in mice.¹⁸

Alteration of the intestinal microbiota has been shown in experimental and clinical inflammatory bowel diseases, allergies, diabetes, and obesity.^{13,38-42} This study provides several lines of evidence that suggest a close association between dysbiosis and GVHD. Mice without GVHD maintained normal microbiota after BMT, and dysbiosis only occurred in mice with GVHD, independent of the murine models used. The normal intestinal environment was never restored as long as severe GVHD persisted, but was restored when tolerance was induced after transplant. In mice with GVHD, the degree of changes to the microflora was significantly correlated to GVHD severity and MHC disparity between the donor and recipient. Furthermore, modifying enteric flora by oral administration of antibiotics inhibited the outgrowth of *E coli* and ameliorated GVHD. The flora shift toward the widespread prevalence of gram-negative bacteria increases the translocation of LPS, the major component of the outer membrane of gram-negative bacteria, into systemic circulation and further accelerates GVHD by stimulates production of inflammatory cytokines, such as TNF- α and IL-1, which are critical effector molecules that mediate GVHD.^{22,43-45} Thus, GVHD and the dysbiosis can lead to a positive feedback loop that increases the translocation of LPS, thereby resulting in further cytokine production, progressive intestinal injury, and systemic GVHD acceleration. Earlier seminal studies in the 1960s-1970s suggested that GVHD is reduced in germfree mice or by treatment with poorly absorbable antibiotics.³⁻⁶ A recent study also demonstrated that modifying the enteric flora using a probiotic microorganism reduced GVHD in mice.⁴⁶ Thus, our study again highlights an important role of oral antibiotics administration on GVHD. Our study demonstrated that dominant bacteria in the intestinal microbiota cause systemic infection. There was a microbiologic evidence of infection in mice with severe GVHD and a correlation between severity of infection and GVHD, thus suggesting that severe bacteremia, probably caused by the translocation of enteric bacteria, can also contribute to GVHD mortality, as previously suggested.^{6,46} Indeed, septicemia by gram-negative rods

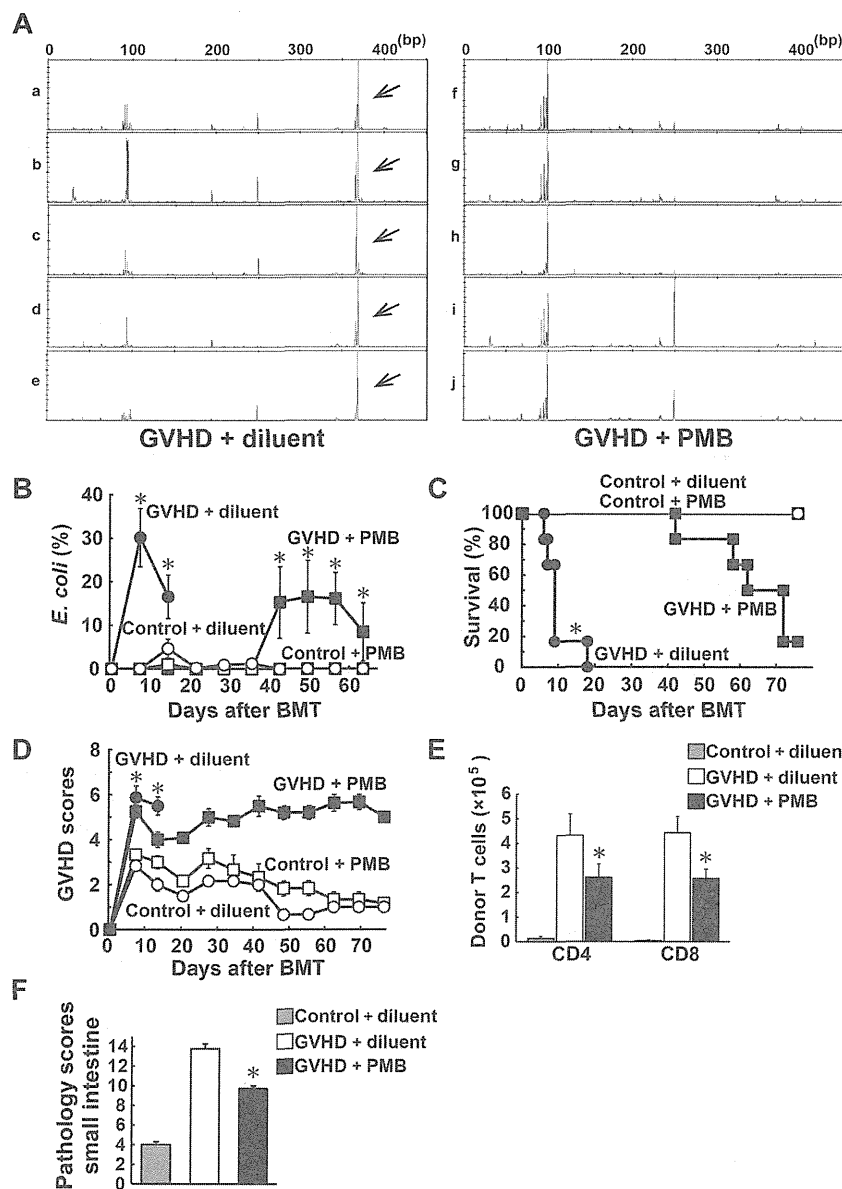


Figure 7. Oral administration of polymyxin B ameliorated GVHD. Lethally irradiated B6D2F1 mice were transplanted with 5×10^6 TCD BM without or with 2×10^6 T cells from B6 or B6-Ly5.1 (CD45.1⁺) donors. Polymyxin B (PMB; 100 mg/kg) or diluent was administered by daily oral gavage from day -4 until day 28 after BMT. (A) Fecal pellets were collected once per week after BMT and intestinal microflora was characterized by RFLP analysis of 16S rDNA genes constructed from each sample of fecal pellets and digested with *HhaI*. Representative RFLP patterns are shown in mice with GVHD receiving diluent (a-e) and those with PMB (f-j) 7 days after BMT. Arrows indicate an OTU for *E. coli*. (B) Time course changes in the proportion of *E. coli* ($n = 6-12$ /group). Survival (C) and clinical GVHD scores (D, mean \pm SE) after BMT are shown ($n = 6-12$ /group). Data from 2 independent experiments were combined. (E) Numbers of donor (CD45.1⁺) T cells in mLN on day 5 ($n = 20$ /group). (F) Pathology scores of the small intestine on day 7 ($n = 20$ /group). Data from 3 independent experiments were combined and are shown as mean \pm SE (* $P < .05$).

is one of the most frequent causes of death in patients with severe intestinal GVHD.

There are other interfaces that exist between the environment and the host, such as the skin and airways. Epithelial cells in these tissues can also release antimicrobial peptides such as β -defensins in response to bacteria and LPS.⁴⁷ GVHD-mediated epithelial cell damage of these tissues may also impair the local secretion of antimicrobial peptides, leading to aberrant overgrowth of pathogens and development of dermal infections or pneumonia, which are frequently observed in patients with GVHD. Furthermore, the development of these pathologic conditions may be associated with the unique tissue specificity of GVHD for tissues that are in contact with high microbial loads, such as the skin, liver, intestine, and lung.

Intestinal epithelial cells are continuously regenerated from ISC, which are required to regenerate damaged sections of the intestinal epithelium.⁴⁸ Paneth cells are derived from ISCs and serve as a niche for ISCs.⁸ Our previous⁷ and current studies addressed intestinal GVHD at the cellular level, and demonstrated that ISCs and their niche Paneth cells could survive pretransplant

conditioning and regenerate injured epithelium by conditioning in the absence of GVHD. However, both ISCs and Paneth cells are targeted by GVHD, resulting in an impairment of the physiologic repair mechanisms of injured epithelium, although it remains to be elucidated whether Paneth cell loss is induced by direct cytotoxicity to Paneth cell itself or secondary to the loss of ISCs. This phenomenon may explain the prolonged and refractory nature of clinical intestinal GVHD. These new insights will help to establish new therapeutic strategies that can be used to prevent and treat GVHD and related infections and improve the clinical outcome of allogeneic BMT.

Acknowledgments

This study was supported by grants from Japan Society for the Promotion of Science (JSJP) KAKENHI (23659490 to T.T., 23390193 to T.A., and 22592029 to K.N.), Health and Labor Science Research Grants (T.T.), the Foundation for Promotion of Cancer Research (Tokyo, Japan; to T.T.), the Knowledge Cluster, Sapporo Bio-S from Ministry of

Education, Culture, Sports, Science and Technology (MEXT; Tokyo, Japan; to T.A.), Yakult Bio-Science Foundation (Tokyo, Japan; to Y.E.), and SENSHIN Medical Research Foundation (to T.T.).

Authorship

Contribution: Y.E. and T.T. developed the conceptual framework of the study, designed the experiments, conducted studies, analyzed

data, and wrote the paper; S.T., H.O., S. Shimoji, K.N., H.U., S. Shimoda, and H.I. conducted experiments; and N.S., T.A., and K.A. supervised experiments.

Conflict-of-interest disclosure: The authors declare no competing financial interests.

Correspondence: Takanori Teshima, Center for Cellular and Molecular Medicine, Kyushu University Hospital, 3-1-1 Maidashi, Higashi-ku, Fukuoka 812-8582, Japan; e-mail: tteshima@cancer.med.kyushu-u.ac.jp.

References

- Bossaer JB, Hall PD, Garrett-Mayer E. Incidence of vancomycin-resistant enterococci (VRE) infection in high-risk febrile neutropenic patients colonized with VRE. *Support Care Cancer*. 2010; 19(2):231-237.
- Winston DJ, Gale RP, Meyer DV, Young LS. Infectious complications of human bone marrow transplantation. *Medicine*. 1979;58(1):1-31.
- van Bekkum D, Vos O. Treatment of secondary disease in radiation chimaeras. *Int J Radiat Biol*. 1961;3:173-181.
- Jones JM, Wilson R, Bealmeas PM. Mortality and gross pathology of secondary disease in germ-free mouse radiation chimeras. *Radiation Res*. 1971;45(3):577-588.
- van Bekkum DW, Roodenburg J, Heidt PJ, van der Waaij D. Mitigation of secondary disease of allogeneic mouse radiation chimeras by modification of the intestinal microflora. *J Nat Cancer Inst*. 1974;52(2):401-404.
- Heit H, Heit W, Kohne E, Fliedner TM, Hughes P. Allogeneic bone marrow transplantation in conventional mice: I. Effect of antibiotic therapy on long term survival of allogeneic chimeras. *Blut*. 1977;35(2):143-153.
- Takahashi S, Kadowaki M, Aoyama K, et al. The Wnt agonist R-spondin1 regulates systemic graft-versus-host disease by protecting intestinal stem cells. *J Exp Med*. 2011;208(2):285-294.
- Sato T, van Es JH, Snippert HJ, et al. Paneth cells constitute the niche for Lgr5 stem cells in intestinal crypts. *Nature*. 2011;469(7330):415-418.
- Selsted ME, Harwig SS. Determination of the disulfide array in the human defensin HNP-2. A covalently cyclized peptide. *J Biol Chem*. 1989; 264(7):4003-4007.
- Ganz T, Selsted ME, Lehrer RI. Defensins. *Eur J Haematol*. 1990;44(1):1-8.
- Salzman NH, Hung K, Haribhai D, et al. Enteric defensins are essential regulators of intestinal microbial ecology. *Nat Immunol*. 2010;11(1):76-83.
- Eckburg PB, Bik EM, Bernstein CN, et al. Diversity of the human intestinal microbial flora. *Science*. 2005;308(5728):1635-1638.
- Qin J, Li R, Raes J, et al. A human gut microbial gene catalogue established by metagenomic sequencing. *Nature*. 2010;464(7285):59-65.
- Hill DA, Artis D. Intestinal bacteria and the regulation of immune cell homeostasis. *Ann Rev Immunol*. 2010;28:623-667.
- Zoetendal EG, Akkermans AD, De Vos WM. Temperature gradient gel electrophoresis analysis of 16S rRNA from human fecal samples reveals stable and host-specific communities of active bacteria. *Appl Environ Microbiol*. 1998;64(10): 3854-3859.
- Kurokawa K, Itoh T, Kuwahara T, et al. Comparative metagenomics revealed commonly enriched gene sets in human gut microbiomes. *DNA Res*. 2007;14(4):169-181.
- Hooper LV, Macpherson AJ. Immune adaptations that maintain homeostasis with the intestinal microbiota. *Nature Rev Immunol*. 2010;10(3):159-169.
- Heimesaat MM, Nogai A, Bereswill S, et al. MyD88/TLR9 mediated immunopathology and gut microbiota dynamics in a novel murine model of intestinal graft-versus-host disease. *Gut*. 2010; 59(8):1079-1087.
- Ubeda C, Taur Y, Jenq RR, et al. Vancomycin-resistant Enterococcus domination of intestinal microbiota is enabled by antibiotic treatment in mice and precedes bloodstream invasion in humans. *J Clin Invest*. 2010;120(12):4332-4341.
- Cooke KR, Kobzik L, Martin TR, et al. An experimental model of idiopathic pneumonia syndrome after bone marrow transplantation. I. The roles of minor H antigens and endotoxin. *Blood*. 1996;88: 3230-3239.
- Asakura S, Hashimoto D, Takahashi S, et al. Alloantigen expression on non-hematopoietic cells reduces graft-versus-leukemia effects in mice. *J Clin Invest*. 2010;120(7):2370-2378.
- Teshima T, Ordemann R, Reddy P, et al. Acute graft-versus-host disease does not require alloantigen expression on host epithelium. *Nat Med*. 2002;8(6):575-581.
- Ayabe T, Satchell DP, Wilson CL, Parks WC, Selsted ME, Ouellette AJ. Secretion of microbicidal alpha-defensins by intestinal Paneth cells in response to bacteria. *Nat Immunol*. 2000;1(2): 113-118.
- Li F, Hullar MA, Lampe JW. Optimization of terminal restriction fragment polymorphism (TRFLP) analysis of human gut microbiota. *J Microbiol Methods*. 2007;68(2):303-311.
- Hayashi H, Takahashi R, Nishi T, Sakamoto M, Benno Y. Molecular analysis of jejunal, ileal, caecal and recto-sigmoidal human colonic microbiota using 16S rRNA gene libraries and terminal restriction fragment length polymorphism. *J Med Microbiol*. 2005;54(Pt 11):1093-1101.
- Simpson EH. Measurement of diversity. *Nature*. 1949;163:688.
- Shannon C. A mathematical theory of communication. *Bell System Technol J*. 1948;27:379-423.
- Ouellette AJ, Hsieh MM, Nosek MT, et al. Mouse Paneth cell defensins: primary structures and antibacterial activities of numerous cryptdin isoforms. *Infect Immun*. 1994;62(11):5040-5047.
- Masuda K, Sakai N, Nakamura K, Yoshioka S, Ayabe T. Bactericidal activity of mouse alpha-defensin cryptdin-4 predominantly affects non-commensal bacteria. *J Innate Immun*. 2011;3(3): 315-326.
- Liu WT, Marsh TL, Cheng H, Forney LJ. Characterization of microbial diversity by determining terminal restriction fragment length polymorphisms of genes encoding 16S rRNA. *Appl Environ Microbiol*. 1997;63(11):4516-4522.
- Hayashi H, Sakamoto M, Benno Y. Phylogenetic analysis of the human gut microbiota using 16S rDNA clone libraries and strictly anaerobic culture-based methods. *Microbiol Immunol*. 2002; 46(8):535-548.
- Ivanov II, Atarashi K, Manel N, et al. Induction of intestinal Th17 cells by segmented filamentous bacteria. *Cell*. 2009;139(3):485-498.
- Shlomchik WD, Couzens MS, Tang CB, et al. Prevention of graft versus host disease by inactivation of host antigen-presenting cells. *Science*. 1999;285(5426):412-415.
- Vaishnava S, Behrendt CL, Ismail AS, Eckmann L, Hooper LV. Paneth cells directly sense gut commensals and maintain homeostasis at the intestinal host-microbial interface. *Proc Natl Acad Sci U S A*. 2008; 105(52):20858-20863.
- Mastroianni JR, Ouellette AJ. Alpha-defensins in enteric innate immunity: functional Paneth cell alpha-defensins in mouse colonic lumen. *J Biol Chem*. 2009;284(41):27848-27856.
- Hooper LV, Midtvedt T, Gordon JI. How host-microbial interactions shape the nutrient environment of the mammalian intestine. *Annu Rev Nutr*. 2002;22:283-307.
- Bäckhed F, Ley RE, Sonnenburg JL, Peterson DA, Gordon JI. Host-bacterial mutualism in the human intestine. *Science*. 2005;307(5717):1915-1920.
- Ley RE, Turnbaugh PJ, Klein S, Gordon JI. Microbial ecology: human gut microbes associated with obesity. *Nature*. 2006;444(7122):1022-1023.
- Turnbaugh PJ, Ley RE, Mahowald MA, Magrini V, Mardis ER, Gordon JI. An obesity-associated gut microbiome with increased capacity for energy harvest. *Nature*. 2006;444(7122):1027-1031.
- Manichanh C, Rigottier-Gois L, Bonnaud E, et al. Reduced diversity of faecal microbiota in Crohn's disease revealed by a metagenomic approach. *Gut*. 2006;55(2):205-211.
- Bollyky PL, Bice JB, Sweet IR, et al. The toll-like receptor signaling molecule Myd88 contributes to pancreatic beta-cell homeostasis in response to injury. *PLoS One*. 2009;4(4):e5063.
- Penders J, Thijs C, van den Brandt PA, et al. Gut microbiota composition and development of atopic manifestations in infancy: the KOALA Birth Cohort Study. *Gut*. 2007;56(5):661-667.
- Hill GR, Ferrara JL. The primacy of the gastrointestinal tract as a target organ of acute graft-versus-host disease: rationale for the use of cytokine shields in allogeneic bone marrow transplantation. *Blood*. 2000;95(9):2754-2759.
- Nestel FP, Price KS, Seemayer TA, Lapp WS. Macrophage priming and lipopolysaccharide-triggered release of tumor necrosis factor alpha during graft-versus-host disease. *J Exp Med*. 1992;175:405-413.
- Cooke KR, Gerbitz A, Crawford JM, et al. LPS antagonism reduces graft-versus-host disease and preserves graft-versus-leukemia activity after experimental bone marrow transplantation. *J Clin Invest*. 2001;107(12):1581-1589.
- Gerbitz A, Schultz M, Wilke A, et al. Probiotic effects on experimental graft-versus-host disease: let them eat yogurt. *Blood*. 2004;103(11):4365-4367.
- Bals R, Wang X, Meegalla RL, et al. Mouse beta-defensin 3 is an inducible antimicrobial peptide expressed in the epithelia of multiple organs. *Infect Immun*. 1999;67(7):3542-3547.
- Sato T, Vries RG, Snippert HJ, et al. Single Lgr5 stem cells build crypt-villus structures in vitro without a mesenchymal niche. *Nature*. 2009; 459(7244):262-265.

blood

2012 120: 4058-4067
Prepublished online September 18, 2012;
doi:10.1182/blood-2012-02-408864

Engulfment of hematopoietic stem cells caused by down-regulation of CD47 is critical in the pathogenesis of hemophagocytic lymphohistiocytosis

Takuro Kuriyama, Katsuto Takenaka, Kentaro Kohno, Takuji Yamauchi, Shinya Daitoku, Goichi Yoshimoto, Yoshikane Kikushige, Junji Kishimoto, Yasunobu Abe, Naoki Harada, Toshihiro Miyamoto, Hiromi Iwasaki, Takanori Teshima and Koichi Akashi

Updated information and services can be found at:
<http://bloodjournal.hematologylibrary.org/content/120/19/4058.full.html>

Articles on similar topics can be found in the following Blood collections
Phagocytes, Granulocytes, and Myelopoiesis (378 articles)

Information about reproducing this article in parts or in its entirety may be found online at:
http://bloodjournal.hematologylibrary.org/site/misc/rights.xhtml#repub_requests

Information about ordering reprints may be found online at:
<http://bloodjournal.hematologylibrary.org/site/misc/rights.xhtml#reprints>

Information about subscriptions and ASH membership may be found online at:
<http://bloodjournal.hematologylibrary.org/site/subscriptions/index.xhtml>

Blood (print ISSN 0006-4971, online ISSN 1528-0020), is published weekly by the American Society of Hematology, 2021 L St, NW, Suite 900, Washington DC 20036.
Copyright 2011 by The American Society of Hematology; all rights reserved.



Engulfment of hematopoietic stem cells caused by down-regulation of CD47 is critical in the pathogenesis of hemophagocytic lymphohistiocytosis

Takuro Kuriyama,¹ Katsuto Takenaka,¹ Kentaro Kohno,² Takuji Yamauchi,¹ Shinya Daitoku,¹ Goichi Yoshimoto,³ Yoshikane Kikushige,¹ Junji Kishimoto,⁴ Yasunobu Abe,⁵ Naoki Harada,³ Toshihiro Miyamoto,¹ Hiromi Iwasaki,² Takanori Teshima,² and Koichi Akashi^{1,2}

¹Department of Medicine and Biosystemic Science, Kyushu University Graduate School of Medical Sciences, Fukuoka, Japan; ²Center for Cellular and Molecular Medicine, Kyushu University Hospital, Fukuoka, Japan; ³Department of Hematology, Kyushu Medical Center, Fukuoka, Japan; ⁴Digital Medicine Initiative, Kyushu University, Fukuoka, Japan; and ⁵Department of Medicine and Bioregulatory Science, Kyushu University Graduate School of Medical Sciences, Fukuoka, Japan

Hemophagocytic lymphohistiocytosis (HLH) is characterized by deregulated engulfment of hematopoietic stem cells (HSCs) by BM macrophages, which are activated presumably by systemic inflammatory hypercytokinemia. In the present study, we show that the pathogenesis of HLH involves impairment of the antiphagocytic system operated by an interaction between surface CD47 and signal regulatory protein α (SIRPA). In HLH patients, changes in expression levels and HLH-specific polymorphism of SIRPA

were not found. In contrast, the expression of surface CD47 was down-regulated specifically in HSCs in association with exacerbation of HLH, but not in healthy subjects. The number of BM HSCs in HLH patients was reduced to approximately 20% of that of healthy controls and macrophages from normal donors aggressively engulfed HSCs purified from HLH patients, but not those from healthy controls in vitro. Furthermore, in response to inflammatory cytokines, normal HSCs, but not progenitors or mature

blood cells, down-regulated CD47 sufficiently to be engulfed by macrophages. The expression of prophagocytic calreticulin was kept suppressed at the HSC stage in both HLH patients and healthy controls, even in the presence of inflammatory cytokines. These data suggest that the CD47-SIRPA antiphagocytic system plays a key role in the maintenance of HSCs and that its disruption by HSC-specific CD47 down-regulation might be critical for HLH development. (*Blood*. 2012;120(19):4058-4067)

Introduction

Hemophagocytic lymphohistiocytosis (HLH) is a syndrome with excessive immune activation characterized by deregulated engulfment of hematopoietic cells by macrophages in the BM. Patients with HLH display hemophagocytosis, pancytopenia, and various inflammatory symptoms, including high fever, acute liver failure, and splenomegaly.^{1,4} HLH is classified into primary HLH and secondary HLH. Primary HLH, also known as familial hemophagocytic lymphohistiocytosis, shows clear familial inheritance or genetic causes, including mutations in the perforin (PRF1), MUNC13-4, syntaxin 11 (STX11), and RAB27A genes.⁵⁻⁹ In primary HLH, natural killer cells and/or cytotoxic T lymphocytes fail to eliminate the targets in response to inflammatory reactions, and the resulting sustained inflammatory responses induce deregulated activation of macrophages. In secondary HLH, macrophages are activated in association with infections and malignant disorders.⁴ The key pathogenic feature of HLH is hypercytokinemia including IFN- γ , TNF- α , IL-6, and M-CSF, which may activate macrophages to engulf blood cells.³ These cytokines are produced mainly by natural killer cells and cytotoxic T lymphocytes, and might stimulate BM macrophages to engulf erythrocytes, leukocytes, platelets, and their precursors in the BM.

The question is, if hypercytokinemia causes activation of macrophages to engulf blood cells, why does such activation occur specifically in BM macrophages and induce severe hypocellularity

and pancytopenia? Engulfment is triggered by the binding of specific receptors on macrophages to their ligands. Receptors on macrophages include phosphatidylserine receptors and low-density lipoprotein-related protein (LRP).¹⁰⁻¹⁴ Lipopolysaccharide and calreticulin (CRT) are typical ligands for these macrophage receptors to induce a prophagocytic signal.^{14,15} The phosphatidylserine-phosphatidylserine receptor system predominantly serves as a prophagocytic signal for macrophages during apoptosis.^{13,16} In contrast, the CRT-LRP system also works on viable cells,¹⁴ so there must be a mechanism to prevent inadequate engulfment of viable cells. Self-recognition to prevent phagocytosis is regulated by the CD47 and signal regulatory protein α (SIRPA) interaction, and CD47-SIRPA signaling plays an important role in preventing phagocytosis of cells.^{17,18} Therefore, phagocytosis of viable cells is regulated by the balance of prophagocytic CRT-LRP and antiphagocytic CD47-SIRPA signals for macrophages, indicating that the balance of this signaling is deregulated in HLH.

CD47 is a member of the Ig superfamily that is ubiquitously expressed in hematopoietic and nonhematopoietic cells.^{17,18} CD47 interacts with SIRPA through its respective IgV-like domains.¹⁸ In contrast, SIRPA is a transmembrane protein that contains 3 Ig-like domains within the extracellular region. SIRPA is expressed in macrophages, myeloid cells, and neurons.¹⁸⁻²¹ The cytoplasmic region of SIRPA has immunoreceptor tyrosine-based inhibitory

Submitted February 5, 2012; accepted August 26, 2012. Prepublished online as *Blood* First Edition paper, September 18, 2012; DOI 10.1182/blood-2012-02-408864.

The online version of this article contains a data supplement.

The publication costs of this article were defrayed in part by page charge payment. Therefore, and solely to indicate this fact, this article is hereby marked "advertisement" in accordance with 18 USC section 1734.

© 2012 by The American Society of Hematology

motifs.¹⁸ Binding cell-surface CD47 with SIRPA on macrophages provokes inhibitory signals through phosphorylation of the immunoreceptor tyrosine-based inhibitory motifs of SIRPA, activating inhibitory tyrosine phosphatases such as SHP1 and SHP2.¹⁸ This signaling inhibits myosin assembly of macrophages, thereby inhibiting phagocytosis.¹⁸ The CD47-SIRPA self-recognition system is primarily used in RBC clearance to maintain homeostasis of the blood.²²

Interestingly, this system also plays a critical role in engraftment of hematopoietic stem cells (HSCs) in xenotransplantation. Transplantation of the BM of CD47-deficient mice could not rescue lethally irradiated wild-type mice,²³ probably due to engulfment of CD47-deficient HSCs by BM macrophages that constitute the HSC niche.^{24,25} In addition, we have reported previously that polymorphism of the SIRPA IgV domain can modulate the binding affinity of mouse SIRPA to human CD47 and plays a decisive role in xenotransplantation of human HSCs into mice; NOD, a mouse line known to have very efficient engraftment of human hematopoiesis, has a SIRPA polymorphism that can recognize human CD47, and this binding produces inhibitory signaling for mouse macrophages not to engulf human HSCs.²⁶

These previous data led us to hypothesize that the BM-specific macrophage activation in HLH is caused by disruption of the CD47-SIRPA self-recognition system. In the present study, we show that in HLH, inflammatory cytokines down-regulate CD47, especially at the HSC stage, which can provoke the engulfment of HSCs by macrophages.

Methods

Patients and samples

Supplemental Table 1 (available on the *Blood* Web site; see the Supplemental Materials link at the top of the online article) summarizes the clinical characteristics of the patients. During the period from October 2005 to April 2011, 24 patients were diagnosed with HLH. The diagnosis of HLH was made according to HLH-2004 diagnostic guideline²⁷ and Tsuda-97.²⁸ The median age was 36 years (range, 16-71). Etiologies were documented in 12 patients: EBV (n = 7), CMV (n = 1), diffuse large B-cell lymphoma (n = 1), EBV⁺ diffuse large B-cell lymphoma (n = 1), defective PRF1 (n = 1), and adult onset Still disease (n = 1). The median hemoglobin level was 11.1 g/dL (range, 6.2-16.2), the median platelet count was $54.8 \times 10^9/L$ (range, 4-187), and the median ferritin level was 4530 ng/mL (range, 620-44 020). Prednisolone-based treatment was used in 14 patients (58%), and HSC transplantation was performed in 2 patients (8%). BM and peripheral blood samples were obtained from healthy volunteers (n = 50) and HLH patients (n = 24). Cord blood samples from full-term deliveries and normal BM samples from normal volunteers were obtained based on informed consent (provided by Kyushu Block Red Cross Blood Center, Japan Red Cross Society). Informed consent was received for all donors in accordance with the Declaration of Helsinki. The institutional review board of Kyushu University Hospital approved all experiments in this study.

Cell lines

A human acute promyelocytic leukemia cell line, NB4, which retains t(15;17), was obtained from the German Collection of Microorganisms and Cell Cultures (DSMZ). NB4 cells were cultured in RPMI 1640 medium (Wako) containing 10% FBS (ICN).

Sequence alignment of the human SIRPA IgV domains

Genomic DNA was extracted by using QIAamp DNA Blood Mini Kit (QIAGEN). The coding region of the SIRPA IgV domain was amplified by PCR. Genomic DNA was used as a PCR template in the following

conditions: 10 minutes at 94°C, 30 cycles of 1 minute at 94°C, 1 minute at 60°C, 1 minute at 72°C, and 16 minutes at 72°C. PCR and sequencing primers were as follows: forward primer 5'-GCCTGCTTC-TGGTGTGCATCCAGTC-3' reverse primer 5'-GAGTTACTGTC-ACAAACCAGAGGC-3'. PCR products were cloned to the PCR 2.1-TOPO vector (Invitrogen) and 10-25 clones were sequenced for every sample.

Abs, cell staining, and sorting

For analysis of cell-surface expression of SIRPA, we used SIRPA mAb (MBL International) and FITC-conjugated antimouse IgG (Beckman Coulter). For analysis of cell-surface expression of CD47, we used PE-conjugated anti-CD47 (BD Pharmingen). For sorting and analysis of CD34⁺CD38⁻ and CD34⁺CD38⁺ cells, cells were stained with FITC-conjugated anti-CD34 (BD Pharmingen), PE-conjugated anti-CRT (Enzo Life Sciences), peridinin chlorophyll A protein-cy5.5-conjugated anti-CD47 (BD Pharmingen), and allophycocyanin-conjugated anti-CD38 (BD Pharmingen). For some experiments, cells were stained with allophycocyanin-conjugated anti-CD34, PE-conjugated anti-CD47, and PE-Cy7 conjugated anti-CD38 (all BD Pharmingen). Before sorting and analysis, lineage cells in cord blood cells were depleted using a lineage cell depletion kit (Miltenyi Biotec). CD34⁺CD38⁻ and CD34⁺CD38⁺ cells were purified on a FACSAria cell sorter (BD Biosciences).

The analysis procedures of CD34⁺CD38⁺ progenitor populations were described previously.^{29,30} BM mononuclear cells were first stained with PE-Cy5-conjugated lineage Abs, including anti-CD3, anti-CD4, anti-CD8, anti-CD10, anti-CD19, anti-CD20, anti-CD14, anti-CD56, and glycophorin A (BD Pharmingen). Subsequently, cells were stained with FITC-conjugated anti-CD34 (BD Pharmingen), PE-conjugated anti-CD47 (BD Pharmingen), PE-Cy7-conjugated anti-CD123 (eBiosciences), and Pacific Blue-conjugated anti-CD45RA (Beckman Coulter) Abs. HSCs, common myeloid progenitors, granulocyte/macrophage progenitors, and megakaryocyte/erythrocyte progenitors were isolated as Lin⁻CD34⁺CD38⁻, Lin⁻CD34⁺CD38⁺CD123⁺CD45RA⁻, Lin⁻CD34⁺CD38⁺CD123⁺CD45RA⁺, and Lin⁻CD34⁺CD38⁺CD123⁻CD45RA⁻ populations. The cells were analyzed and sorted with a FACSCalibur flow cytometer and a FACSAria 2 cell sorter (both BD Biosciences). The mean fluorescent intensity of CD47 and CRT was normalized and shown as a ratio to PBMCs from healthy donors.

Preparation of human macrophages from peripheral blood

Monocytes were purified from PBMCs by positive selection using MACS CD14 Micro Beads (Miltenyi Biotec). These cells were incubated with X-VIVO10 (Lonza) containing 2% AB serum and 100 ng/mL of M-CSF (R&D Systems) for more than 96 hours to obtain macrophages.^{31,32}

In vitro phagocytosis assays for target cells

Peripheral blood-derived macrophages were prepared and incubated at 1.0×10^4 cells in 200 μ L of RPMI 1640 medium in Falcon culture tubes (2058; BD Biosciences), and then 1.0 - 5.0×10^4 target cells were added to the tubes and incubated at 37°C for 2 hours. Before the addition of target cells to macrophage-containing tubes, cells were opsonized with CD34 Ab (sc-19621; Santa Cruz Biotechnology) for CD34⁺CD38⁻ cells and CD34⁺CD38⁺ cells isolated from normal and HLH BM by FACS sorting; CD13 Ab (sc-51522; Santa Cruz Biotechnology) and CD33 Ab (sc-19660; Santa Cruz Biotechnology) for NB4 cells; CD45 Ab (555480; BD Pharmingen) for lymphocytes; and neutrophils and glycophorin A Ab for RBCs (555569; BD Pharmingen). For activation of macrophages, cells were incubated with IFN- γ (100 ng/mL; R&D Systems) for 24 hours and with lipopolysaccharide (0.3 μ g/ μ L) for 1 hour, and then harvested and washed 3 times with PBS before the addition of target cells. After coinubation with macrophages and target cells, they were mounted on cytospin preparations, and 1000 macrophages were tested to enumerate engulfing ones by a blinded observer. We calculated the phagocytic index using the following formula: phagocytosis index = phagocytic macrophages/number of macrophages.³³

Inhibition of CD47 expression by siRNA

To investigate the effect on phagocytosis according to the expression level of CD47, CD47 expression of NB4 cells and CD34⁺ cord blood cells was down-regulated using siRNA. CD47 siRNA primers used were as follows: siRNA1, UAUACACGCCGCAAUACAGAGACUC and GAGUCUCU-GUAUUGCGGCGUGUAUA; siRNA2, UAGAAGUCACAAUUAAC-CAAGGCC and GGCCUUGGUUUAAUUGUGACUUCUA. The Nucleofector kit V and Human CD34 Cell Nucleofector kit (both Amaxa) were used to transfect siRNA and transfected NB4 cells, and lineage-depleted cord blood cells were incubated for 48 and 24 hours, respectively. NB4 cells and CD34⁺CD38⁻ cells were then sorted depending on CD47 expression using the FACSaria 2 cell sorter (BD Biosciences), and these cells were used for in vitro phagocytic assays to determine the phagocytic index.

Quantitative RT-PCR

Total RNA was extracted from normal and HLH BM. Reverse transcription was performed using a high-capacity cDNA reverse transcription kit (Applied Biosystems) according to the manufacturer's instructions. CD47 and control gene 18srRNA primers were obtained from Applied Biosystems. Amplification, detection, and quantification were performed with the TaqMan ABI Prism 7000 sequence detection system (Applied Biosystems). Data were calculated by the relative quantitation method ($\Delta\Delta Ct$) compared with 18srRNA as an internal control.

Measurement of cytokines by ELISA

Cytokines, including IFN- γ , TNF- α , IL-6, and M-CSF, from HLH and normal blood serum were measured with ELISA. IFN- γ was measured with the IFN- γ Quantikine ELISA kit (DIF50; R&D Systems), TNF- α was measured with the TNF- α Quantikine HS ELISA kit (HSTA00D; R&D Systems), IL-6 was measured with the IL-6 Quantikine ELISA kit (D6050; R&D Systems), and M-CSF was measured with the M-CSF Quantikine ELISA kit (DMC00B; R&D Systems).

In vitro treatment of normal HSCs with inflammatory cytokines

To evaluate the effects of inflammatory cytokines on the expression level of CD47, lineage-depleted cord blood cells were purified by negative selection using the MACS lineage cell depletion kit (Miltenyi Biotec) and cultured in 24-well dish (3047; BD Biosciences) with 300 μ L of X-VIVO10 supplemented with 10% FBS and cytokines as follows: SCF (50 ng/mL; R&D Systems), M-CSF (750 pg/mL; R&D Systems), IL-6 (200 pg/mL; R&D Systems), TNF- α (20 pg/mL; R&D Systems), and IFN- γ (250 pg/mL; R&D Systems). After 24 hours of culture, CD34⁺CD38⁻ and CD34⁺CD38⁺ cells were sorted with the FACSaria 2 cell sorter (BD Biosciences), and these cells were used to determine the phagocytic index.

Statistical analysis

Statistical analysis was performed using jmp Version 9 software (SAS Institute). CD47 expression on CD34⁺CD38⁻ cells, CD34⁺CD38⁺ cells, and bulk among the groups were compared with the Dunnett test. For siRNA experiments using NB4 cells and CD34⁺CD38⁻ cells, phagocytic index was compared with a conventional *t* test. For phagocytic assays using CD34⁺CD38⁻ cells from cord blood cells that had been cultured with inflammatory cytokines, *P* values were obtained by ANCOVA. *P* < .05 was considered statistically significant.

Results

Changes in expression levels of SIRPA or SIRPA mutations do not occur in HLH patients

Several variants of the IgV domain in SIRPA (exon3 of SIRPA), where the CD47-binding site is located, have been reported in human.^{26,34} We first tested the possibility that the SIRPA polymorphism may influence the development of HLH. We examined the

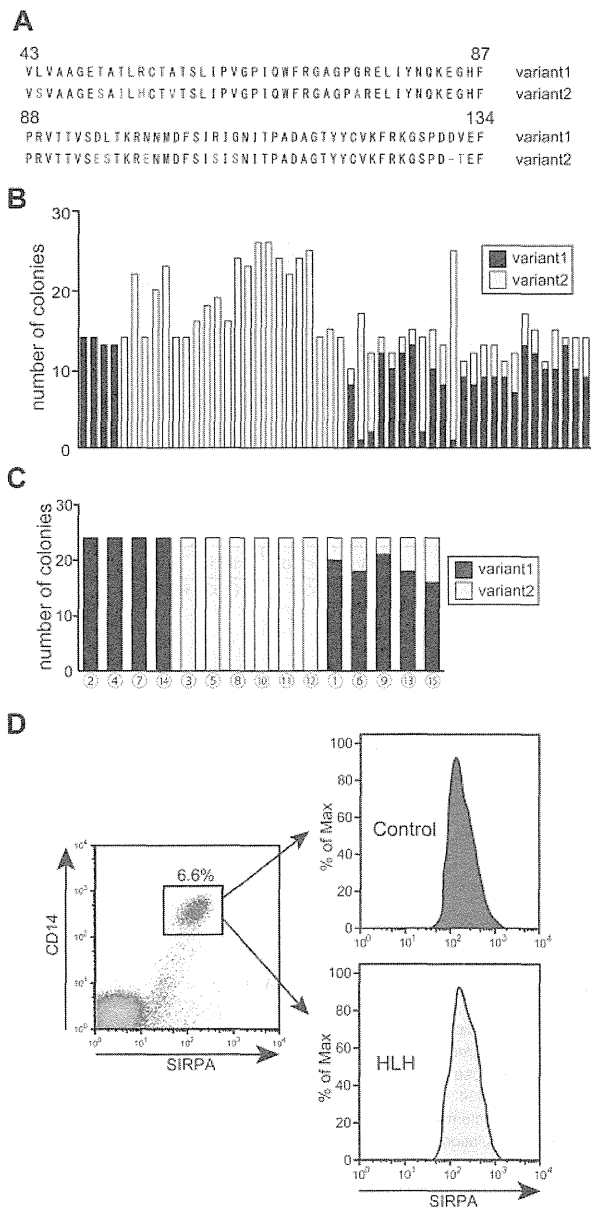


Figure 1. SIRPA mutation or changes of its expression level is not involved in pathogenesis of HLH. (A) Sequence alignment of SIRPA IgV domains (exon 3 of SIRPA) identified by sequence analysis from genomic DNA of 50 healthy donors. Two variants, which we have described previously,²⁰ were identified in the present study. There are 13 amino acid differences between these 2 variants. (B) Distribution of genotype of SIRPA IgV domains in 50 healthy donors. PCR products were cloned to pCR 2.1-TOPO vector and 10-25 clones were sequenced for every sample: 24 were heterozygous for variants 1 and 2, 4 were homozygous for variant 1, and 22 were homozygous for variant 2. (C) Distribution of genotype of SIRPA IgV domains in 15 HLH patients (unique patient number [UPN] 1-15); 4 (UPN 2, 4, 7, and 14) were heterozygous for variants 1 and 2, 6 (UPN 3, 5, 8, 10, 11, and 12) were homozygous for variant 1, and 5 (UPN 1, 6, 9, 13, and 15) were homozygous for variant 2. There were no other variants or changes of SIRPA IgV domain in HLH patients. (D) Representative expression of surface SIRPA on CD14⁺ cells of control and HLH patients on FACS. There was no significant difference in the expression level of SIRPA in CD14⁺ monocytes between HLH and normal BM: The mean \pm SD of CD47 fluorescence intensity was 116 \pm 1.7 and 118 \pm 9.6 in healthy controls (n = 5) and HLH patients (n = 5), respectively (*P* = .88).

sequence alignment of SIRPA IgV domain of 50 Japanese healthy donors. Although many polymorphisms have been reported previously in the SIRPA IgV domain,²⁶ we identified 2 variants (variants 1 and 2) in the present study (Figure 1A). There are 13 amino acid differences between these 2 variants as we have described,²⁶ and

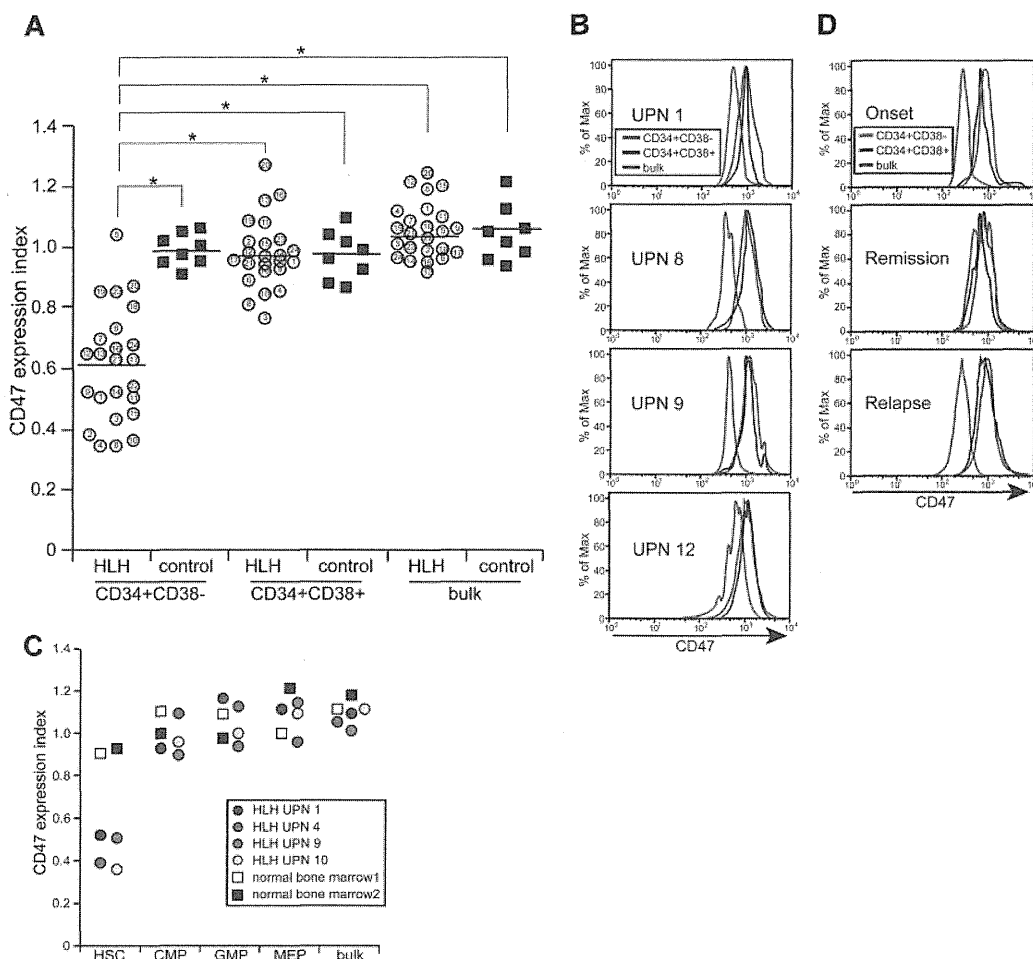


Figure 2. CD47 expression is down-regulated specifically in the CD34⁺CD38⁻ HSC fraction in HLH patients, reflecting the disease activity. (A) CD47 expression of CD34⁺CD38⁻ cells, CD34⁺CD38⁺ cells and unfractionated BM cells in HLH patients and healthy controls. The number in each open circle corresponds to the unique patient number (UPN) of patients (supplemental Table 1). The horizontal bars in each group show mean values of the group. The level of CD47 on CD34⁺CD38⁻ cells was significantly decreased compared with that on CD34⁺CD38⁺ cells and more mature cells. The CD47 expression index represents the relative surface CD47 level (median CD47 levels of analyzed cells/those in normal blood mononuclear cells). (B) Histograms of CD47 expression of BM cells in 4 representative HLH patients (UPN 1, 8, 9, and 12). (C) CD47 expression of CD34⁺CD38⁻ HSC-enriched fraction and of each progenitor cell fraction in HLH patients (UPN 1, 4, 9, and 10) and healthy controls. All progenitor populations expressed equivalent levels of CD47, and CD47 expression was down-regulated only in HSC fraction. (D) Change of CD47 expression in UPN 10 during multiple episodes of HLH. Down-regulation of CD47 repeatedly occurred at exacerbation of HLH.

their binding capacity to CD47 was equal.³⁴ Twenty-four of 50 healthy donors were heterozygous for variants 1 and 2, 4 were homozygous for variant 1, and 22 were homozygous for variant 2 (Figure 1B). Similarly, we examined sequence alignment of SIRPA IgV domain of 15 HLH patients, in whom we identified variant 1 and variant 2 SIRPA IgV-encoding alleles, but no other variants or changes in the allele burden of variants 1 and 2 (Figure 1C). Furthermore, the expression level of SIRPA on the cell surface did not differ among HLH and normal BM cells (data not shown) and CD14⁺ cells (Figure 1D). These data suggest that alterations in SIRPA or its expression are not involved in the pathogenesis of HLH.

CD47 is down-regulated in the CD34⁺CD38⁻ HSCs from HLH patients

We also evaluated the expression level of CD47 in the BM of HLH patients. As shown in Figure 2A, the control normal BM cells ubiquitously express CD47. Its expression levels were always high in the CD34⁺CD38⁻ fraction that concentrates HSCs,³⁵ in the

CD34⁺CD38⁺ progenitor fraction, and in unfractionated cells that mainly contained mature cells. In the HLH BM, CD47 expression is down-regulated specifically in the CD34⁺CD38⁻ HSC fraction compared with those in the progenitor and mature cell fraction by approximately 2-fold at the expression level (Figure 2A-B). To determine more precisely the expression of CD47 in progenitor fractions, we subfractionated CD34⁺CD38⁺ progenitors into common myeloid progenitor, granulocyte/macrophage progenitor, and megakaryocyte/erythrocyte progenitor populations.²⁹ These progenitors had equivalent levels of CD47 (Figure 2C and supplemental Figure 1). The down-regulation of CD47 occurs in conjunction with the deterioration of HLH. Patient number 10, who suffered from adult onset primary HLH due to defective PRF1,³⁶ had repeated episodes of HLH. The follow-up of this patient revealed that the expression levels of CD47 in HSCs normalized in remission, but its down-regulation occurred again at exacerbation of the disorder (Figure 2D). These data strongly suggest that the HSC stage-specific down-regulation of CD47 plays a critical role in HLH development.

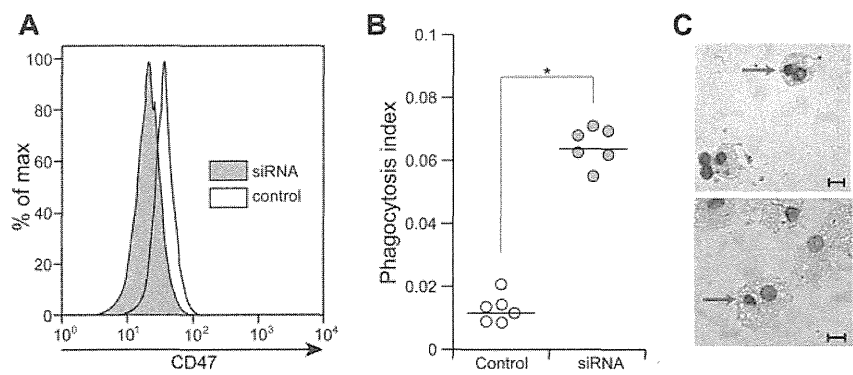


Figure 3. Knocking down CD47 in CD34⁺CD38⁻ cells induces their engulfment by macrophages. (A) Knock-down of CD47 expression in normal CD34⁺CD38⁻ cells by siRNA for human CD47. Treatment of CD34⁺CD38⁻ cells with siRNA for 48 hours induced 60% reduction of CD47 expression in these cells. (B) CD34⁺CD38⁻ cells treated with the siRNA for human CD47 showed accelerated engulfment by normal macrophages. Vertical axis shows the phagocytosis index (phagocytosis index = phagocytic macrophages/number of macrophages) and the bars show mean value. **P* < .01 by conventional *t* test. (C) Engulfment of CD34⁺CD38⁻ cells treated with siRNA by normal macrophages (Giemsa staining). Scale bars indicate 10 μ m.

Reduction of CD47 expression in HSCs in HLH patients results in engulfment of HSCs by macrophages

We also sought to investigate whether CD47 expression levels in target cells affect the efficiency of engulfment by macrophages. We first treated NB4, a human promyelocytic leukemia cell line, with 2 types of siRNAs targeting human CD47. siRNA1 showed a 72% reduction of CD47 expression in NB4 cells, whereas siRNA2 showed a 37% reduction (supplemental Figure 2A). We then quantitated the engulfment of macrophages by enumeration of the phagocytosis index (phagocytic macrophages/number of macrophages).^{22,33,35,37} In the culture of these cells with normal macrophages, rare control NB4 cells were engulfed by macrophages, whereas NB4 cells treated with siRNA1 or siRNA2 showed 5- and 2.5-fold increases in the phagocytosis index, respectively, which illustrates the efficiency of engulfment by macrophages (supplemental Figure 2B). Therefore, the engulfment of NB4 evoked by CD47 suppression occurs in a dose-dependent manner.

We treated purified normal CD34⁺CD38⁻ HSCs with the siRNA1 for 24 hours and evaluated the phagocytosis index. As shown in Figure 3A, an approximately 30% reduction of the level of CD47 expression was observed in purified CD34⁺CD38⁻ cells treated with siRNA1. The CD34⁺CD38⁻ cells treated with siRNA1 became susceptible to phagocytosis, and showed 5.3-fold increase in the phagocytosis index compared with untreated CD34⁺CD38⁻ cells (*P* < .01). Therefore, the reduction of CD47 in CD34⁺CD38⁻ cells stimulates macrophages to engulf these cells.

We also investigated whether HSCs isolated from HLH patients are susceptible to phagocytosis by normal macrophages. We purified CD34⁺CD38⁻ HSCs and CD34⁺CD38⁺ progenitors from HLH patients (patients number 4, 16, and 22) and healthy controls and evaluated the phagocytosis index. As shown in Figure 4A, in all 3 HLH patient samples, CD34⁺CD38⁻ cells with a 40%-60% reduction of CD47 levels (Figure 2A) were actively engulfed by macrophages. In contrast, CD34⁺CD38⁺ cells of HLH patients showed a low phagocytic index, as was also observed in HSCs or progenitors in healthy controls (Figure 4A). Therefore, the efficiency of phagocytosis by macrophages is inversely correlated with the expression of CD47 of target cells even in human HLH samples, showing that a decrease of CD47 expression can induce engulfment of HSCs in HLH, at least in vitro.

Finally, we investigated whether HSCs were engulfed and reduced in number in HLH patients. We counted the number of CD34⁺CD38⁻ cells in BM from healthy controls and HLH patients (Figure 4B). The frequencies of CD34⁺CD38⁻ HSCs were significantly reduced in HLH BM (0.04% \pm 0.02% of total nucleated cells) compared with those in normal adults (0.15% \pm 0.09%). The number of nucleated cells in the BM was also reduced by approximately 50%. As a result, as shown in Figure 4B, the number of CD34⁺CD38⁻ cells in HLH patients was reduced down to only 23% of those in healthy adults. Although the number of CD34⁺CD38⁺ cells were also reduced in the HLH patients (approximately 42% of healthy adults), the reduction was more

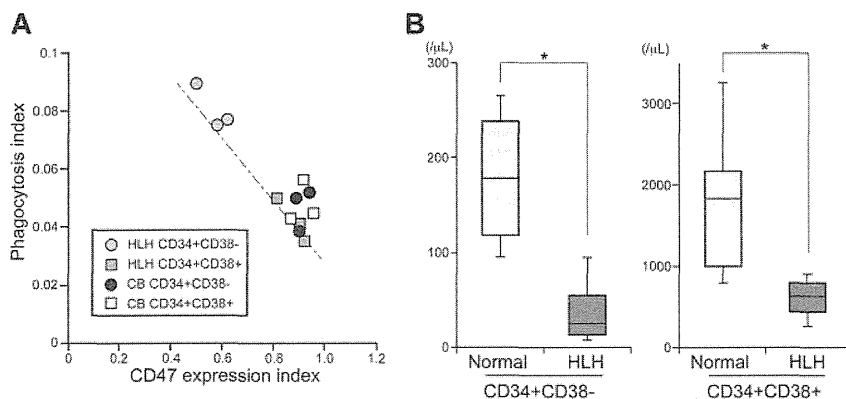


Figure 4. The CD34⁺CD38⁻ HSC fraction but not the progenitor population in HLH patients is sensitive to engulfment by macrophages. (A) Relationship between the level of CD47 expression and the phagocytosis index tested in vitro. CD34⁺CD38⁻ cells and CD34⁺CD38⁺ cells from 3 HLH patients (unique patient number [UPN] 4, 16, and 22) and healthy controls were cultured with activated macrophages. CD47 expression index represents the relative surface CD47 level calculated as the median CD47 levels of analyzed cells/those in normal blood mononuclear cells. The bar shows the regression line; the coefficient of correlation value was -0.91 . (B) The number of CD34⁺CD38⁻ HSCs and CD34⁺CD38⁺ progenitor cells in the BM of HLH patients (*n* = 14) and healthy controls (*n* = 6) are shown in the box and whisker plot. HLH patients had significantly decreased numbers of HSC and progenitor populations, but the magnitude of suppression of HSCs was more profound. The bottom and top of the boxes are the 25th and 75th percentile values. The bands in the middle of the boxes represent the 50th percentile (median). Error bars show 1 SD differences above and below the mean of the data. **P* < .01 by conventional *t* test.

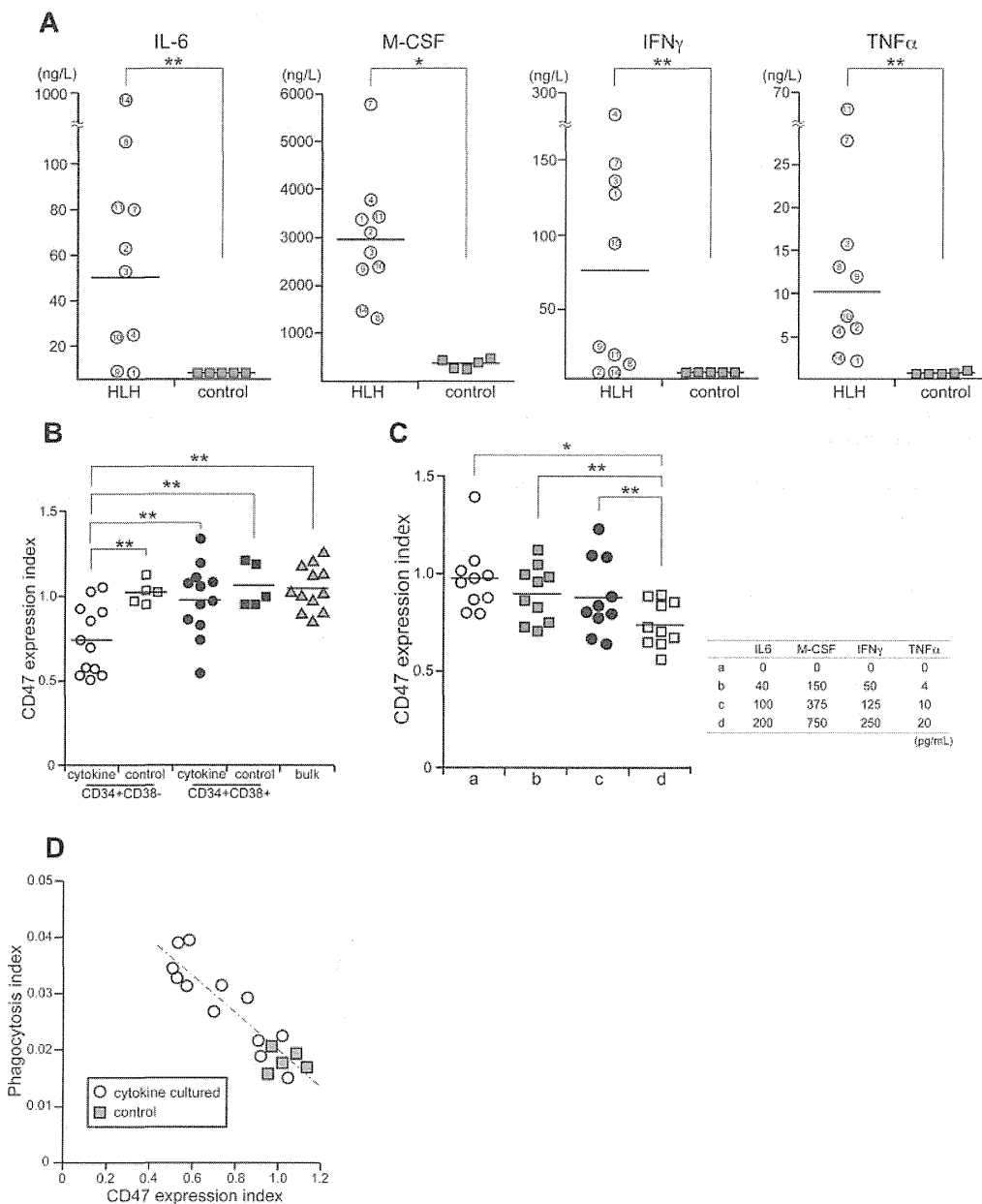


Figure 5. Inflammatory cytokines down-regulate CD47 specifically in CD34⁺CD38⁻ cells to induce engulfment by macrophages. (A) Serum levels of M-CSF, IL-6, TNF- α , and IFN- γ from in patients by ELISA. These cytokines were extremely high in HLH samples compared with healthy controls. * $P < .01$; ** $P < .05$ by conventional t test. (B) Changes of CD47 expression levels in normal CD34⁺CD38⁻ HSCa and CD34⁺CD38⁺ progenitor cells in the presence of inflammatory cytokines. CD47 expression index represents the relative surface CD47 level calculated as median CD47 levels of analyzed cells/those in normal blood mononuclear cells. The HSC fraction, but not the progenitor fraction, showed down-regulated CD47 in response to cytokines. ** $P < .05$ by conventional t test. (C) Suppression of CD47 in CD34⁺CD38⁻ cells by graded doses of inflammatory cytokines. The concentration of inflammatory cytokines is shown on the right. (D) Engulfment of HSCs by macrophages in response to reduction of CD47 expression by cytokines in vitro. The CD47 expression index was inversely correlated with phagocytosis index. The bar shows the regression line; the coefficient of correlation value was -0.89 .

profound in the CD34⁺CD38⁻ fraction. The number of HSCs is reduced in the BM of HLH patient by phagocytosis that is evoked by HSC-specific reduction of CD47.

Inflammatory cytokines down-regulate CD47 expression and enhance the efficiency of engulfment of HSCs by macrophages

It has been shown that hypercytokinemia plays a critical role in the development of HLH. Consistent with previous results,³ HLH patient sera contained high levels of inflammatory cytokines, including IL-6, M-CSF, IFN- γ , and TNF- α (Figure 5A). We

investigated whether these cytokines can affect the expression of CD47 in hematopoietic cells. Lineage-depleted cord blood cells were cultured with M-CSF (750 pg/mL), IL-6 (200 pg/mL), IFN- γ (250 pg/mL), and TNF- α (20 pg/mL) for 24 hours, and CD47 expression was evaluated in stem, progenitor, and mature cell fractions. The concentrations of inflammatory cytokines were compared with those of HLH patient sera. CD47 expression was down-regulated specifically in CD34⁺CD38⁻ HSCs, whereas it did not change in CD34⁺CD38⁺ progenitors or unfractionated mature cells (Figure 5B). The down-regulation of

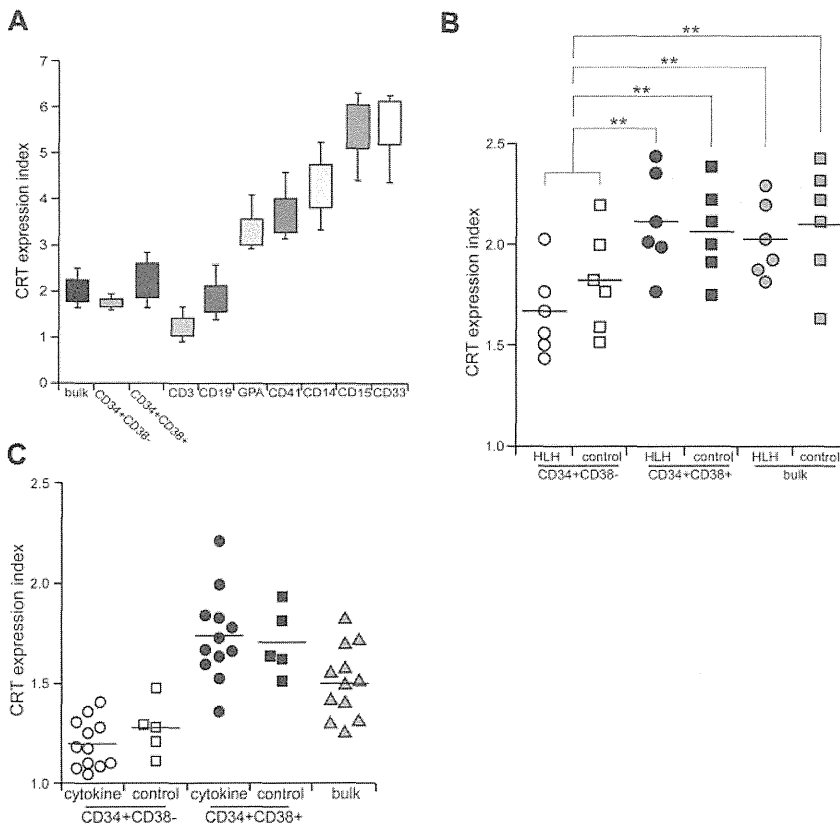


Figure 6. CRT is not involved in the engulfment of HSCs in HLH. (A) CRT expression in normal hematopoietic cells. CRT expression index represents the relative surface CRT level calculated as median CRT levels of analyzed cells/those in normal blood mononuclear cells. Error bars show 1 SD differences. (B) CRT expression in CD34⁺CD38⁻ HSCs, CD34⁺CD38⁺ progenitors, and unfractionated BM cells from HLH patients and healthy controls. The expression level of CRT was equivalent in HLH patients and healthy controls in all of these cell fractions. ***P* < .05 by conventional *t* test. (C) The effect of cytokines on CRT expression. CRT expression was not changed irrespective of incubation with cytokines in any of these cell fractions. Bars show the mean values.

CD47 expression in CD34⁺CD38⁻ cells occurs in response to cytokines in a dose-dependent manner (Figure 5C). The cells treated with cytokines were further tested for phagocytosis assays. As shown in Figure 5D, the expression level of CD47 in CD34⁺CD38⁻ HSCs treated with inflammatory cytokines was inversely correlated with the phagocytosis index. These data suggest that inflammatory cytokines can down-regulate CD47 expression specifically in HSCs, inducing HSC-targeted engulfment by BM macrophages.

CRT, a dominant prophagocytic factor, is down-regulated in CD34⁺CD38⁻ HSCs in both HLH patients and healthy controls

CRT is the major prophagocytic factor expressed on the cell surface, which binds to lipoprotein-related protein on cell surface of macrophages and stimulates their phagocytic activities.¹⁴ During apoptotic cell death, these cells are engulfed due to loss of CD47 expression and coordinated up-regulation of cell-surface CRT as the dominant prophagocytic signal.³⁸ We evaluated the expression level of CRT in stem, progenitor, and mature cell fractions in HLH patients. In the healthy BM, CRT was highly expressed in mature myeloid cells, but at a very low level in lymphoid cells. Erythroblasts and megakaryocytes expressed intermediate levels of CRT. Interestingly, the expression level of CRT was very low in immature hematopoietic cells, including CD34⁺CD38⁻ HSCs and CD34⁺CD38⁺ progenitor cell fractions (Figure 6A). CD34⁺CD38⁻ HSCs expressed even lower levels of CRT compared with those in CD34⁺CD38⁺ progenitors (Figure 6B). In HLH patients, the expression of CRT was comparable to that in healthy controls: The CD34⁺CD38⁻ HSC population expressed only a very low level of CRT (Figure 6B). We then cultured normal HSCs in the presence of inflammatory cytokines including M-CSF, IL-6, IFN- γ , and TNF- α

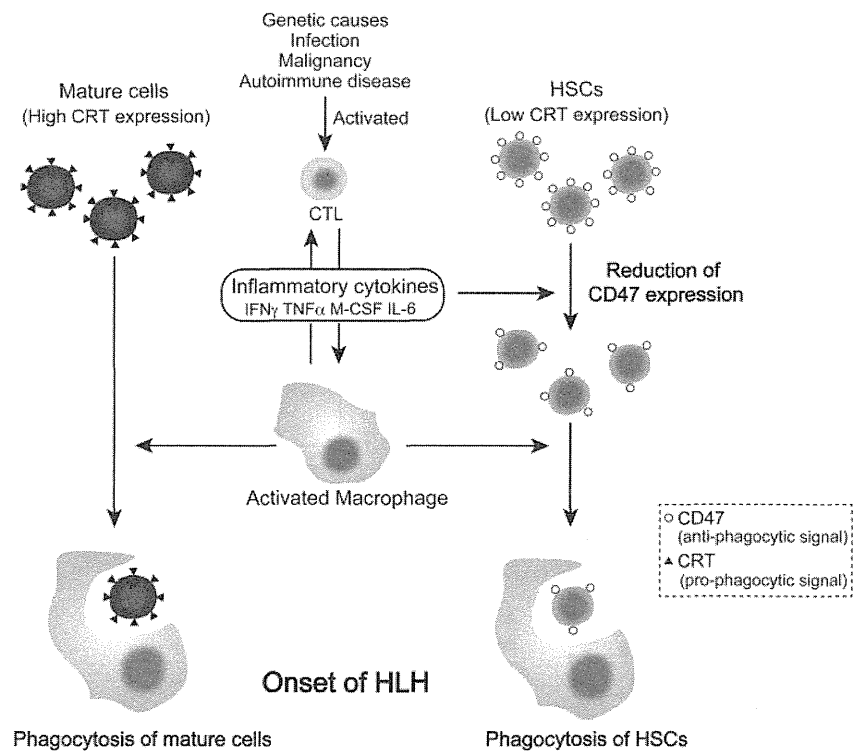
for 24 hours, and the expression of CRT did not change in the HSC or progenitor populations (Figure 6C). Therefore, CRT is shut down at the HSC stage even in HLH patients, suggesting that the expression of CRT is not involved in engulfment of HSCs by macrophages.

Discussion

In HLH, cytopenia occurs in more than 80% of patients at disease presentation. The BM may present either hypocellularity or hypercellularity at the onset, but eventually becomes hypoplastic. This phenotype is thought to result mainly from suppression of hematopoiesis by elevated inflammatory cytokines such as TNF- α and IFN- γ and from engulfment of hematopoietic cells by BM macrophages.³⁹ The serum concentrations of these cytokine levels in HLH are usually quite higher than those with sepsis,⁴⁰ suggesting that these extremely high levels of cytokines should be critical in the pathogenesis of HLH. In the present study, we show that HLH patients have low numbers of HSCs, and that HSCs from HLH patients down-regulate CD47 and are prone to be engulfed by macrophages more actively than normal HSCs. We also show that inflammatory cytokines can down-regulate the expression of CD47 selectively in HSCs, resulting in a disruption of self-recognition based on the CD47-SIRPA system to induce engulfment of HSCs by macrophages. Based on these data, we propose that the disruption of the CD47-SIRPA system plays a primary role in the development of HLH.

Macrophages function to clear foreign, aged, or damaged cells via phagocytosis, and this process is regulated by the balance between antiphagocytic and prophagocytic signals. The primary

Figure 7. Pathogenesis of HLH based on antiphagocytic and prophagocytic signaling. In HLH, cytotoxic T lymphocytes are activated by genetic abnormality, infection, malignancy, and autoimmune disease, and then produce inflammatory cytokines and activate macrophages. Activated macrophages engulf mature cells such as RBCs, platelets, and granulocytes, which are susceptible to phagocytosis because of high expression of prophagocytic CRT. In contrast, inflammatory cytokines suppress hematopoiesis by their direct toxic effects and down-regulate CD47 expression on HSCs, resulting in a decreased threshold of antiphagocytic signals. Therefore, HSCs were engulfed by activated macrophages, causing the BM of HLH patients to become hypoplastic, thereby exacerbating pancytopenia.



antiphagocytic and prophagocytic signals for macrophages to engulf nonapoptotic cells are the CD47-SIRPA and the LPR-CRT systems, respectively.¹⁴ Because in the present study, freshly isolated HSCs from HLH patients, but not from healthy controls, were engulfed by macrophages *in vitro* (Figure 4A), the balancing of this signaling should be altered in HLH.

Many polymorphisms have been detected in human SIRPA, especially in the ligand-binding IgV domain.²⁶ In the present study, however, HLH patients did not have any specific polymorphisms of SIRPA. In addition, we could not find differences in the level of SIRPA expression between normal and HLH BM cells. We conclude that neither polymorphisms of SIRPA nor the change of its expression levels are involved in the pathogenesis of HLH.

Conversely, the expression of CD47 was significantly down-regulated specifically in the HSC fraction in HLH patients, but was not changed in progenitors and other mature cells (Figure 2A-C). The expression level of CD47 in HLH HSCs was approximately 50% at the protein level compared with that in normal HSCs. This level of reduction readily induced macrophage activation *in vitro* (supplemental Figures 2 and 4A). BM HSCs in HLH patients were reduced in number, presumably by engulfment, but were functionally normal, at least in terms of colony-forming capabilities *in vitro* (supplemental Figure 1B). The down-regulation of CD47 in HLH HSCs might be induced by high levels of serum inflammatory cytokines such as IL-6, M-CSF, IFN- γ , and TNF- α , because incubation of normal HSCs, but not progenitors, with these cytokines induced down-regulation of CD47 *in vitro* in a dose-dependent manner (Figure 5B-C), and rendered normal HSCs susceptible to engulfment by macrophages (Figure 5D).

It remains unclear by what mechanism only the HSC fraction is sensitive to cytokines to down-regulate CD47. Interestingly, in contrast to the CD47 protein, the CD47 mRNA levels were normal in HSCs in all 5 HLH patients analyzed by quantitative real-time PCR assays (not shown), so the down-regulation of CD47 could occur at the posttranscriptional level. In a recent study, Junker et al

examined miRNA profiles from active and inactive lesions in multiple sclerosis patients, and found out that miRNA-34a, miRNA-155 and miRNA-326, the targets of which include human CD47, were up-regulated in active sclerosis lesions.⁴¹ These miRNAs reduce the expression of CD47 in brain-resident cells, promoting macrophages to engulf myelin. In the present study, we evaluated miRNA-34a, miRNA-155, and miRNA-326 expression in HSCs in HLH patients, but could not find any differences in the expression level of these miRNAs in HSCs from HLH patients and healthy controls (T.K., unpublished data, February 2010). Inflammatory cytokines did not induce the increased expression of these miRNAs (T.K., unpublished data, March 2010). It is critical to clarify the mechanism of CD47 down-regulation in the HSC fraction in future studies.

The expression of CRT on the cell surface is an important prophagocytic signal. When CRT binds to LPR on macrophages, LPR signaling immediately can stimulate macrophages to engulf the CRT-expressing cells.^{14,15} This “eat me” signal could antagonize the “do not eat me” signal mediated by the CD47-SIRPA interaction.⁴² Once apoptosis is initiated, CRT is up-regulated, phosphatidylserine is exposed to the cell surface, and CD47-SIRPA signaling is rendered ineffective, thereby permitting engulfment of target cells.⁴² In contrast to CD47, which is ubiquitously expressed in normal hematopoietic cells from HSCs to mature cell stages (Figure 2A), CRT is expressed mainly in myeloerythroid cells, but only at a low level in immature CD34⁺CD38⁻ HSCs. Because recent studies have shown that macrophages are cellular components of HSC niches,²⁴ down-regulation of CRT might be required for HSCs to stay intact at the niche. In contrast, mature myeloerythroid cells might be primed to be prophagocytic via sustained CRT expression, which enables macrophages to engulf these cells on activation by, for example, cytokines.

Previous studies have shown that the CD47-SIRPA system is critical to engraftment and maintenance of HSCs *in vivo*. We have reported that the reason that human HSCs engraft efficiently in the